University of Texas Rio Grande Valley
ScholarWorks @ UTRGV

Theses and Dissertations

7-2020

# The Rotational Spectrum of 1,1-Diiodoethane

Michael Joseph Carrillo
*The University of Texas Rio Grande Valley*

Follow this and additional works at: https://scholarworks.utrgv.edu/etd

Part of the Chemistry Commons

## Recommended Citation

Carrillo, Michael Joseph, "The Rotational Spectrum of 1,1-Diiodoethane" (2020). *Theses and Dissertations*. 629.
https://scholarworks.utrgv.edu/etd/629

This Thesis is brought to you for free and open access by ScholarWorks @ UTRGV. It has been accepted for inclusion in Theses and Dissertations by an authorized administrator of ScholarWorks @ UTRGV. For more information, please contact justin.white@utrgv.edu, william.flores01@utrgv.edu.

# THE ROTATIONAL SPECTRUM OF 1,1-DIIODOETHANE

A Thesis

by

MICHAEL JOSEPH CARRILLO

Submitted to the Graduate college of
The University of Texas Rio Grande Valley
In partial fulfillment of the requirements for the degree of

MASTER OF SCIENCE

July, 2020

Major Subject: Chemistry

# THE ROTATIONAL SPECTRUM OF 1,1-DIIODOETHANE

A Thesis
by
MICHAEL JOSEPH CARRILLO

COMMITTEE MEMBERS

Dr. Wei Lin
Committee Chair

Dr. Shervin Fatehi
Committee Member

Dr. Evangelia Kotsikorou
Committee Member

Dr. Erik Plata
Committee Member

Dr. Arnulfo Mar
Committee Member

July, 2020

Copyright 2020 Michael Joseph Carrillo

All Rights Reserved

# ABSTRACT

Carrillo, Michael J. The Rotational Spectrum of 1,1-diiodoethane. Master of Science (MS), July, 2020, 78 pp., 8 tables, 19 figures, references, 45 titles.

The first chapter of this thesis introduces the basic theory of rotational spectroscopy. This includes the theory of a rigid rotor, centrifugal distortion, and hyperfine effects. The theory behind diatomic systems is explained first, and then expanded to the asymmetric top system. The second chapter encompasses a brief overview on the development of microwave spectroscopy and discusses the instruments that were utilized during this study, namely the cavity-based and chirped-pulse Fourier transform microwave spectrometers. Chapter three describes the quantum chemical calculation methods and basis sets that were applied throughout this study. Chapter four discusses the progress of data analysis of the rotational spectrum of 1,1-diiodoethane. Only a few molecules with two iodine atoms have been studied using rotational spectroscopy. This is due to the complex hyperfine splitting structure arising from the presence of two iodine nuclei. The analysis was aided by quantum chemical calculations. A potential energy surface scan was performed at the MP2/aug-cc-pVTZ-pp level to acquire the lowest energy conformation of 1,1-diiodoethane and to help estimate the $V_3$ barrier height. *Ab initio* calculations were carried out on the global minimum conformation at the CCSD(T) and MP2 levels along with the aug-cc-pVTZ-pp basis set, in order to help predict the molecular geometry and the hyperfine parameters. We report the high resolution rotational spectroscopic observation of the 1,1-diiodoethane for the first time. The spectrum was observed at 11-18 GHz frequency range in a jet-pulsed cavity-based Fourier transform microwave spectrometer. The observed transition frequencies were analyzed to yield the rotational constants, centrifugal distortion constants, the nuclear quadrupole coupling constants, and nuclear-spin rotation constants. Previous literature shows that molecules with a terminal methyl group may undergo internal rotation. The experimental spectrum of 1,1-diiodoethane seems to indicate that there is internal rotation, however, with our preliminary fit this cannot be concluded for sure.

# DEDICATION

I would like to dedicate this thesis to my loving and caring family, fur-babies, and close friends. To my mother, Marisela Carrillo, my father Joe Carrillo, and my sister Kayla M. Carrillo, I want to say thank you for all the endless love and support throughout this endeavor. I could have not gotten where I am without any of your moral support. To my loving partner Muriah D. Huerta, I cannot thank you enough for the immense loving care and support you have shared with me throughout the years. I can't wait for what the future has in store for us, I love you! To my loving friends J. Patrice N., K. Camila G., and Gabs. R.-C., I thank you for being amazing and caring friends and for being my chosen family, I love you dearly. To my fur-babies, Killian Iodus Carrillo, Biggie Smalls, Andrea 3000, Luna, Niklaus M. Carrillo, Chlorus Carrillo, Trixie Carrillo, and my eldest Sammy Carrillo I dedicate this and everything I will ever do for you. To my best friend Tania V. Alvarez, thank you for all these years that you have shared with me. I cannot wait for the many more. I will never ever take our friendship for granted. Thank you for everything, I love you! To my grandparents, I love you and would like for you to always know I could not have done this without your unconditional support. Para mis abuelitos, Rosendo y Guadalupe Rodriguez, Fidel y Magdalena Carrillo, les doy gracias por todo el apoyo que me an dado en todo mi vida. Los amo muchisimo!

# ACKNOWLEDGMENTS

There is an immense amount of people I would like to thank throughout this journey. I will do my best to include everyone, as you are all instrumental to my achievements. First and foremost, I would like to thank my whole family. I thank you for helping me realize (a little late) that I wanted to obtain my doctorates in chemistry, and I will not stop until I have achieved this.

I would like to thank Professor Wei Lin, whom I could never ever thank enough for all that you have done for me. You are the best mentor and friend I could have ever had. I am so happy that I was able to be your graduate student and undergraduate student. I learned so much from you even when you had to explain things 1 million times over. Thank you for all the patience, love, and support. Thank you for allowing me to run wild with my ideas. I really appreciate that. You have inspired me to want to obtain my Ph.D. even more than ever, as you are the best mentor anyone can ever have. I want to aspire to be a mentor like you. You will always have a place in my heart, thank you for everything Professor Lin. To the students in Professor Lin's laboratory, be past, present, or future that includes, Agapito Serrato III, Patrice Niduaza, David Vera, Karla Salazar, Diego Rodriguez, Joely Gonzalez, Alitza Gracia, Zayra Gonzalez, Alex Treviño, Tania V. Alvarez, Juan Baltierrez, Rick Luna, and those of you who are coming in later, thank you for everything. I will always hold you deep in my heart and mind. I would also like to thank all my Professors in the Department of Chemistry at the University of Texas Rio Grande Valley. Firstly, Professor Shervin Fatehi, whom always made the time to discuss and teach me about theories way over my head. Thanks for always helping me by providing knowledge that was an integral part in not only my academic career, but in my daily life. To the students in Professor Fatehi's group, which includes and is not limited to, Daniel Piñon and Catherine Clark thank you for the kind words and many teachings. May we collaborate sometime in the future. To Professor Evangelia Kotsikorou, thank you for molding me with your teachings and kind advice throughout the years. Thank you teaching me about the other side of computational chemistry. I really appreciated the classes. To Professor Arnulfo Mar, I want to thank you for helping me throughout my undergraduate year and graduate years. I will never ever forget the metabolic cycles, as it is important to our everyday life. To Professor Jason Parson, thank you for teaching me about x-ray and instrumentation. Those were always interesting classes. To professor Erik Plata thanks for showing me about the $SN_1$ and $SN_2$ reactions by using G16. I found it very useful for reaction pathways that are relevant in my research. To Professors Yunjie Xu, and Wolfgang Jäger, whom are at the University of Alberta, Canada. Thank you for inviting me to your laboratory with open arms and teaching me how to operate my first chirped-pulse and cavity-based FTMW spectrometers. I look back on that memory so much. May we collaborate on other projects together in the future. I would also like to thank Professors Elijah G. Schnitzler and Professor Javix Thomas, whom were part of the group at the time we were carrying out experiments.

I would also like to say thank you to Professor Yuan-Pern Lee for financial support and for inviting me to your laboratory at the National Chiao Tung University in Hsinchu, Taiwan. It was an amazing experience to learn so much about the *para*-hydrogen matrix technique and collaborate with you. I would also like to thank Professor Lee's group members, Sharon Tsao, Rita Ji, Pavithraa Sundararajan, Zhong Chenan/ Bruce (鍾晨安), Cai Shiyi/ Sam (蔡釋頤), Cai

Huiru/Flora (蔡蕙如), Su Xuanxuan/ Iris (蘇瑢瑄), and Tina for making my experience so awesome. To professor Karolina A. Haupa, thank you for teaching me a plethora of information in spectroscopy, computational chemistry, and for taking me on trips everywhere to beautiful places in Taiwan. You are a fantastic friend that I hope to see again, hopefully at ISMS. I really enjoyed all the late night talks, jamming to heavy metal in the middle of the night, and conducting experimentation until the devils hour. I can’t wait to work in your lab in the future. To Piotr Kotlinski, thanks for being such an amazing friend! I cannot stress how humble and full of life you are. I appreciated all the experiences we had together. I would like to thank Professor Effat (Fariba) Jokar for being an amazing friend, I can only wish you the best. I can’t wait to see you soon!

Professor Yasuki Endo at the National Chiao Tung University, thank you so much for giving me the opportunity to conduct research in your laboratory. Thank you for also helping me assign my first molecule with two nuclear magnetic moments. Thanks for allowing me to witness radical species and the use of double resonance within our experiments. I was blown away by the work we conducted in our research. I was more blown away that you were able to assign the microwave spectrum of $CO_2$. Thanks for everything professor, I admire you so much for it.

To Professor Stephen Kukolich, thank you for inviting me to your laboratory at the University of Arizona. I finally got to see the largest microwave spectrometer in the world it was a sight to see. I also want to say thanks to Professor Adam Daily for helping me understand how to approach analysis and teaching me about other programs to autofit microwave spectrums. To Zunwu Zhou, I cannot thank you enough for all the help you provided while we were conducting experimental search for our molecule. I hope all went well with you Ph.D. thesis defense.

*“Do or do not, there is no try!” ~Master Yoda~*

# TABLE OF CONTENTS

Page

ABSTRACT ... iii

DEDICATION ... v

ACKNOWLEDGMENTS ... vi

TABLE OF CONTENTS ... ix

LIST OF TABLES ... xi

LIST OF FIGURES ... xiii

CHAPTER I. ROTATIONAL SPECTROSCOPY ... 1

- 1.1 Introduction ... 1
- 1.2 Rigid Rotor ... 4
- 1.3 Centrifugal Distortion ... 10
- 1.4 Nuclear Quadrupole Coupling ... 12
- 1.5 Nuclear Spin-Rotation ... 15

CHAPTER II. INSTRUMENTAL ... 18

- 2.1 Introduction ... 18
- 2.2 Cavity-Based FTMW Spectrometer ... 20
- 2.2.1 Fabry-Perot Cavity ... 20
- 2.2.2 Supersonic Expansion ... 22
- 2.2.3 Cavity-Based Fourier Transform Method ... 23
- 2.3 Chirped-Pulse FTMW Spectrometer ... 25
- 2.3.1 Differences of Cavity-Based and Chirped Pulse FTMW Spectrometers ... 25
- 2.3.2 BrightSpec. K-Band FTMW Spectrometer ... 26

CHAPTER III. THEORETICAL CALCULATIONS ... 29

- 3.1 Methods ... 29
- 3.2 *Ab initio* Calculations ... 32
- 3.3 Hartree-Fock Method ... 32
- 3.4 Basis Set ... 34

3.5 Second-Order Møller-Plesset Perturbation Theory ............................................ 35
3.6 Coupled-Cluster Theory.......................................................................................... 38
3.7 Quantum Chemical Calculations and Texas Advanced Computing Center ......... 40
CHAPTER IV. RESULTS..................................................................................................41
4.1 Understanding Alkyl Halides.................................................................................. 41
4.2 *Ab initio* Calculations.................................................................................................. 49
4.3 Internal Rotation ..................................................................................................... 53
4.4 Analysis.................................................................................................................... 55
4.4.1 Sequential coupling Scheme ................................................................................ 57
4.4.2 Consequential Coupling Scheme ........................................................................ 61
4.5 Conclusion .............................................................................................................. 62
REFERENCES ................................................................................................................. 63
APPENDIX A .................................................................................................................. 69
APPENDIX B .................................................................................................................. 72
BIOGRAPHICAL SKETCH ............................................................................................ 78

# LIST OF TABLES

Page

Table 1. Describes different rigid rotors types.................................................................... 9

Table 2. Shows the bond length and bond angles of the methyl and deuterated halides............. 43

Table 3. Shows the bond length (R) and bond angle (A) for the different ethyl halides that have been previously mentioned............................................................ 45

Table 4. Shows the calculated structure parameters of 1,1-diiodoethane at the CCSD(T) and MP2 level. ........................................................................................ 52

Table 5. shows calculated spectroscopic parameters from CCSD(T) and MP2 calculations....... 53

Table 6. Shows the different $V_3$ measured through rotational spectroscopy............................... 55

Table 7. shows the experimental spectroscopic parameters after the sequential fitting.............. 59

Table 8. Observed rotational transition frequencies of the 1,1-diiodoethane.............................. 61

LIST OF FIGURES

Pages

Figure 1. Shows the energy transition for a ground electronic, vibrational, and rotational transition. Schematic not fit to scale. .................... 3

Figure 2. Depicts the moment of inertia of a diatomic molecule, and the bond distance from both atoms. .................... 4

Figure 3. Shows the equally spaced absorption rotational spectrum of a rigid rotor diatomic molecule [12]. .................... 6

Figure 4. shows the oblate and prolate type molecules [14]. .................... 9

Figure 5. Shows the relation of the asymmetric rotor energy levels to the symmetric prolate and oblate tops [15] .................... 10

Figure 6. Shows the conventional waveguide (top) first commercial microwave spectrometer from HP (bottom) [2]. .................... 18

Figure 7. Shows the cavity-based FTMW spectrometer at NCTU (top) and the BrighSpec. chirped-pulse FTMW spectrometer at UTRGV (bottom). .................... 20

Figure 8. The left mirror is the tunable mirror that has the microwave antenna at the center. The right mirror injects the sample under supersonic expansion. .................... 20

Figure 9. Shows the $2_{22}$-$1_{10}$ rotational transition of 1,1-diiodoethane with a Doppler splitting of 53.4 kHz. It also shows a spectrum in the time domain on the left and frequency domain on the right. .................... 22

Figure 10. Shows the pulse nozzle injecting 1,1-diiodoethane [6] .................... 22

Figure 11. Demonstrates microwave radiation being propagated from the microwave antenna, while the sample is injected into the cavity [8] .................................................. 23

Figure 12. Shows the molecular pulse, microwave pulse, and trigger [9]. .................................. 24

Figure 13. Shows the inside of the chamber of Prof. Pate's chirped-pulse FTMW spectrometer [4]. ..................................................................................................... 25

Figure 14. Shows the rotational spectrum of acetic acid at 300 K within 100,000 average shots from 18-26 GHz region produced from the Maria instrument. ........................... 26

Figure 15. Shows the PES scan at MP2/aug-cc-pVTZ-pp level ................................................. 49

Figure 16. Shows 1,1-diiodoethane's calculated from CCSDT/aug-cc-pvtz-pp bond angles and bond lengths (top) along with its inertial axis(bottom). ....................................... 51

Figure 17. Shows a generic $V_3$ potential energy barrier along with the two vibrational states being split. ......................................................................................................... 54

Figure 18. Shows the experimental (top) and predicted (bottom) rotational spectrum of 1,1-diiodoethane with a fitting of 0.7 MHz .............................................................. 57

Figure 19. Shows a zoomed in spectrum of 1,1-diiodoethane. .................................................... 58

# CHAPTER I

# ROTATIONAL SPECTROSCOPY

## 1.1 Introduction

Molecular spectroscopy is the study of how molecules interact with light (radiation). It is conventionally divided into four distinctive frequency regions, electronic (uv-vis), vibrational (infrared), rotational (microwave), and radiofrequency spectroscopy. Electronic spectroscopy is the study of the promotion of electrons from their lowest electronic state to a higher energy electronic state. Electronic spectroscopy deals with mostly visible and ultraviolet frequency. Next is vibrational spectroscopy, which is the study of various vibrations within the molecule. Vibration spectroscopy deals with mostly infrared frequency. Rotational spectroscopy, which studies the rotations of molecules. It deals with microwave frequency. Radiofrequency spectroscopy corresponds to the energy involved in changing the direction of spin of a nucleus, for example, Nuclear Magnetic Resonance (NMR). The first three can be further described in Fig. 1, where the schematic is not fit to scale. Electronic energy is corresponding to the largest energy scale of the three. It is so large that it cannot be shown on paper if scaled. In between the ground and excited electronic energies exist the vibrational energy levels. These energies are equally spaced and are a magnification of the first electronic ground state. They then are further magnified to show the rotational energy, which is the smallest amount in terms of energy. The topic of this thesis will describe rotational spectroscopy.

Microwave (rotational) spectroscopy is an extraordinary technique that studies how matter interacts with microwave radiation. Microwave radiation ranges from 300 MHz – 40 GHz. It probes the rotational motions of molecules in the gas-phase [18]. In order for the rotational spectrum of a molecule to be observed, the molecule must exhibit a dipole moment. A dipole moment arises when two atoms share electrons unequally. The more electronegative atom will pull the shared electron closer to it, resulting in a charge unbalance (polarity). The rotating dipole moment will interact with the microwave radiation. In this chapter, I will introduce some basic theories of the microwave spectroscopy in order to understand the microwave spectrum of 1,1-diiodoethane. I will start with the simpler case of diatomic molecules, then expand into polyatomic molecules. It is not my intention to provide a detailed explanation of microwave (rotational) spectroscopy in this thesis. If the readers would like to obtain more information about rotational spectroscopy, please take a further look at references [18,90,36,60,21,41,96,5,28,46,59,70,29,50,11]

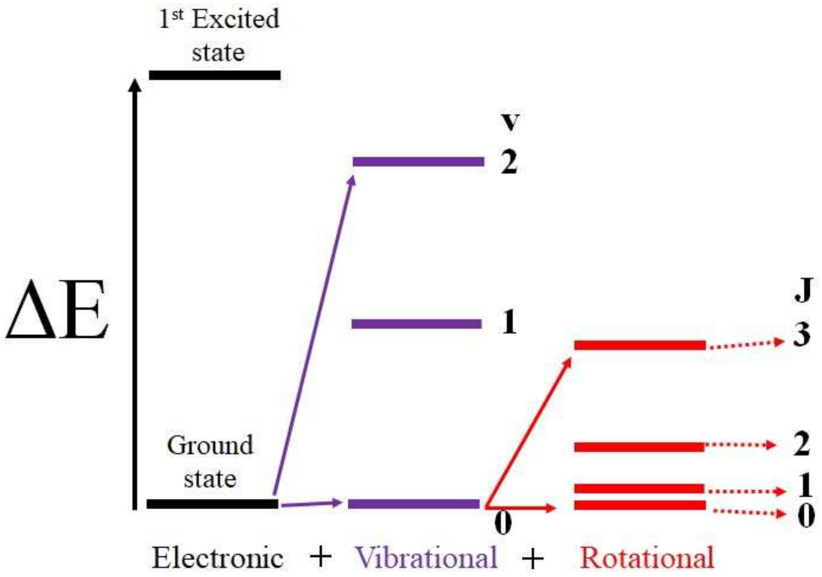

Figure 1. Shows the energy transition for a ground electronic, vibrational, and rotational transition. Schematic not fit to scale.

Quantum chemistry focuses on solving the time-independent Schrödinger's equation, eq. 1 and is composed of

$$\hat{H}\Psi = E\Psi \tag{1}$$

Where the $\hat{H}$ is the Hamiltonian operator and in this case is composed of the kinetic and potential energy of the system, $\Psi$ is the electronic wavefunction that contains dynamic information for the system of study, and *E* is the quantized energy of the system [28]. Eq. 1 is used widely to study many systems. In rotational spectroscopy, the Hamiltonian operator can be described as

$$\hat{H} = \hat{H}_R + \hat{H}_{CD} \tag{2}$$

Where the $\hat{H}_R$ corresponds to the Hamiltonian for the rigid rotor, $\hat{H}_{CD}$ is the Hamiltonian corresponding to the centrifugal distortion. But for molecules like 1,1-diiodoethane, the Hamiltonian becomes further perturbed as shown below

$$\hat{H} = \hat{H}_R + \hat{H}_{CD} + \hat{H}_{NQC} + \hat{H}_{NSR} \tag{3}$$

where $\hat{H}_{NQC}$ is the Hamiltonian for the nuclear quadruple coupling, and $\hat{H}_{NSR}$ represents Hamiltonian for the nuclear spin-rotation, which will be discussed in vivid details later in this chapter.

## 1.2 Rigid Rotor

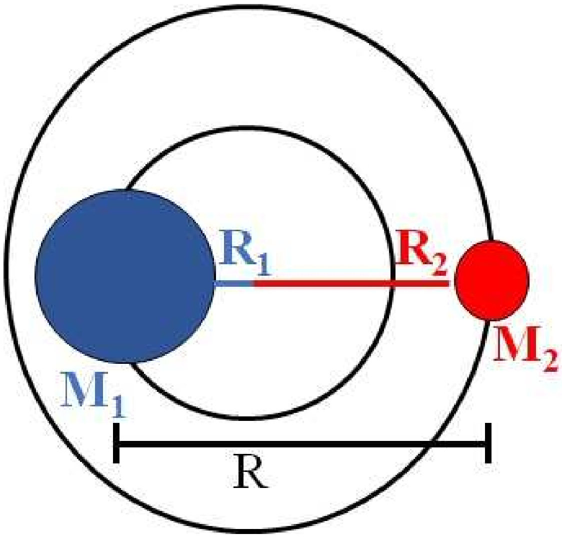

Figure 2. Depicts the moment of inertia of a diatomic molecule, and the bond distance from both atoms.

A diatomic molecule contains a center-of-mass where those two atoms are rotating about as shown in Fig. 2. This center-of-mass is chosen to be the origin of the coordinate system, such as

$$M_1R_1 = M_2R_2 \tag{4}$$

where $M_1$ and $M_2$ are the masses of the atoms and $R_1$ and $R_2$ are the distance from the center-of-mass. The distance of both atoms can be better described by $R = R_1 + R_2$, also defined as bond length. When this is combined and manipulated with eq. 4, we obtain

$$R_1 = \frac{M_2R}{M_1+M_2} \quad \text{and} \quad R_2 = \frac{M_1R}{M_1+M_2} \tag{5}$$

The total kinetic energy of a rotating system is

$$KE = \frac{M_1V_1^2}{2} + \frac{M_2V_2^2}{2} \tag{6}$$

where $V$ is the velocity of that particle and can be translated into $r\omega_{rot}$ since the motion is rotational. Where the rotational angular speed ($\omega_{rot}$) arises from the two atoms in Fig. 2 covering the circumference of the circle per a period of time. The kinetic energy expression becomes

$$KE = \frac{I\omega^2}{2} \tag{7}$$

where $I$ is the moment of inertia and $\omega$ is the angular speed. $I$ can be further transformed into

$$I = \mu R^2 = \frac{M_1 M_2}{M_2 + M_1} R^2 \tag{8}$$

and arises when both parts of eq. 5 are combined. The μ expression in eq. 8 is the reduced mass term and $R$ is the bond length. The classical mechanical expression for angular momentum is known to be $L=I\omega$ and can convert the kinetic energy term into

$$KE = \frac{L^2}{2I} \tag{9}$$

The Hamiltonian operator for a rigid rotor diatomic system can then become

$$\widehat{H}_R = \frac{\hat{J}^2}{2I} \tag{10}$$

where $J$ is the total rotational angular momentum quantum number that arises when we are discussing quantum mechanics [18,90,36,60,21,41,96]. Since in a diatomic system there is only one axis of rotation, it is sufficient to say that the moment of inertia $I_x = I_y$ and $I_z = 0$. When eq. 10 is plugged into eq. 1, the Schrödinger's equation can be solved when $\psi$ is the spherical harmonic $Y_{JM}$. Producing the rotational energy of the system

$$E_J = \frac{\hbar^2}{2I} \mathrm{J}(\mathrm{J}+1) \tag{11}$$

and $\hbar$ is the reduced Planck's constant. If we define the rotational constant B, where B is

$$B = \frac{\hbar^2}{2I} \tag{12}$$

then eq. 11 becomes

$$E_J = BJ(J+1) \tag{13}$$

As seen in eq. 12, the rotational constant B is inversely proportional to the moment of inertia. Therefore, by plugging in the experimental rotational constants, one can determine the moment of inertia. Because the moment of inertia is proportional to the bond length, one can obtain the bond length very accurately for that given diatomic system, as shown in Fig. 2. If the rotational constant(s) for a diatomic molecule is large, then the molecule's molecular mass must be small. Thus, larger molecules will have more closely spaced rotational energy levels and vice versa. For example, carbon monoxide is very light, which would cause the rotational spectrum to be seen in the far-infrared region. For diatomic/linear molecules the rotational spectrum is equally spaced by $2B$ as seen from Fig. 3 [12]. This is because of the selection rule in diatomic/linear molecules which is $\Delta J = \pm 1$ and for rovibronic transitions the $J = 0$ is allowable [60].

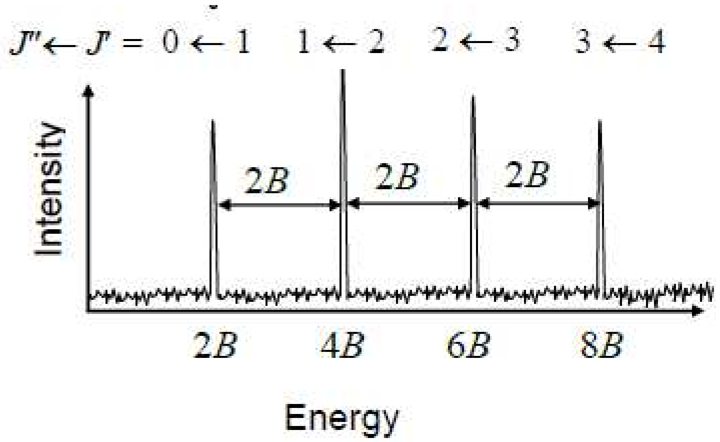

Figure 3. Shows the equally spaced absorption rotational spectrum of a rigid rotor diatomic molecule [70].

That 2*B* spacing originates from molecules rotational energy levels *F(J),* where *F(J)=E(J)/h*, and is denoted as

$$\nu_{J''\rightarrow J'} = F(J)' - F(J)'' \tag{14}$$

Where the *J"* is the initial rotational energy level and *J'* is the final rotational energy level. Fig. 3 shows the general spectrum of a rigid rotor molecule. If the transition is from *J* → *J*+1

$$\nu_{J\rightarrow J+1} = B(J+1)(J+2) - BJ(J+1) = 2B(J+1) \tag{15}$$

Which denotes the 2*B* spacing of the energy levels that are shown in Fig. 3.

For a 3-dimensional molecule, the classical kinetic energy term is now defined as

$$KE = \frac{1}{2}\, I_x\omega_x^2 + \frac{1}{2} I_y\omega_y^2 + \frac{1}{2} I_z\omega_z^2 \tag{16}$$

where $I_x$ and $I_y$ are no longer equal to each other, and $I_z$ does not equal zero. $I_x$, $I_y$, and $I_z$ are the diagonal terms in the moment of inertia tensor. The tensor also has off-diagonal terms that also contribute to the total kinetic energy of the system. It must be noted that the angular speed is also a tensor in the x,y, and z axis. When a molecule is rotating in 3-d space, it is easier to utilize the internal axis system instead of the Cartesian axis system. The benefit of using internal axis system is that it moves with the molecule, where the Cartesian axis system must be recalculated every time the molecule rotates. Therefore eq. 16 can become eq. 17, where

$$KE = \frac{1}{2}\, I_a\omega_a^2 + \frac{1}{2} I_b\omega_b^2 + \frac{1}{2} I_c\omega_c^2 \tag{17}$$

Eq. 17 can be further expanded into

$$KE = \frac{L_a^2}{2I_a} + \frac{L_b^2}{2I_b} + \frac{L_c^2}{2I_c} \tag{18}$$

Which follows the same route as eq. 9. Therefore, we can convert the classical mechanical operator to the quantum mechanical rotational angular momentum quantum number *J*. Producing

$$\hat{H}_R = \frac{\hat{J}_a^2}{2I_a} + \frac{\hat{J}_b^2}{2I_b} + \frac{\hat{J}_c^2}{2I_c} = AJ_a^2 + BJ_b^2 + CJ_c^2 \qquad (19)$$

Where it is made up of the three rotational constants *A, B,* and *C*. For an asymmetric top, $A > B > C$. Meaning that the rotational constant *C* has the largest moment of inertia followed by *B* and finally *A* coming in last with the smallest moment of inertia. When the rotational Hamiltonian is plugged into the Schrödinger's equation, the total rotational energy for a given level becomes

$$E = \frac{1}{2}(A + C)J(J + 1) + \frac{1}{2}(A - C)E_{J_\tau}(\kappa) \qquad (20)$$

Where $E_{J_\tau}(\kappa)$ is an integer and *A* and *C* are rotational constants [18,90].

Molecules belong to different types of rotors (as seen in Table 1). For instance, linear/diatomic molecules follow *B*=*C*, which is experimentally easy to investigate, and is denoted as the 2*B* spacing that was explained above. But for asymmetric tops, the rotational constants are different. *B* no longer is equal to *C*, and there are three different rotational constants now as seen in eq. 20. The experimental spectrum also becomes more complex because it is not following the 2*B* spacing anymore. For instance, the molecule that will be reported in chapter four, 1,1-diiodoethane is an asymmetric top.

| | | |
|---|---|---|
| **Linear/diatomic molecule** | | $B = C$ |
| **Spherical top** | | $A = B = C$ |
| **Symmetric Top** | **Prolate** | $A > B = C$ |
| | **Oblate** | $A = B > C$ |
| **Asymmetric top** | | $A > B > C$ |

Table 1. Describes different rigid rotors types

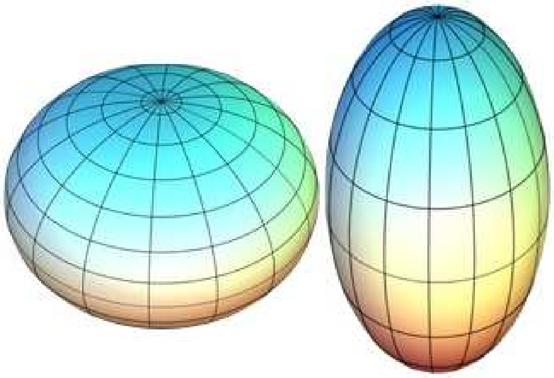

Figure 4. shows the oblate and prolate type molecules [50].

Because asymmetric top molecules can also be considered near-oblate or near-prolate type molecules, eq. 21

$$\kappa = \frac{2B-A-C}{A-C} \tag{21}$$

describes the behavior of the asymmetric rotor. It measures the asymmetry with the rotational constants along their *a, b,* and *c* axes. When κ is -1 (also known as $k_a$) it is more inclined to follow the prolate sketch shown on the left side of Fig.4. When the κ=+1 (also known as $k_c$) it follows the oblate sketch shown on the right side of Fig. 4. When κ =0 it is following a pure asymmetric top type molecule and the energy levels are not degenerate like the symmetric top [90]. The energy levels of an asymmetric top are different from those in the symmetric tops as shown in Fig. 5 [11]. In the case of an asymmetric rotor, there are (2*J*+1) distinct rotational sublevels for every *J* value. Which differs from what is observed in the symmetric top, where the rotational sublevels are (*J*+1) for each *J* value [90].

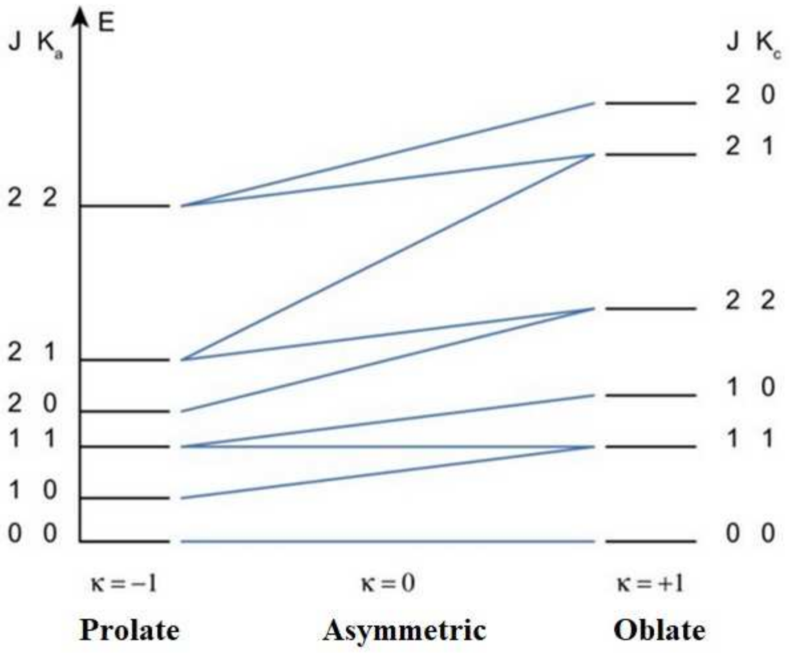

Figure 5. Shows the relation of the asymmetric rotor energy levels to the symmetric prolate and oblate tops [11].

The term κ is also proportional to the $k_a$ and $k_c$ from eq. 22. In other words, as $J$ increase so will κ. Therefore, as asymmetry increases, so will the K splitting, which will not be close to any degenerate $k$ levels of the symmetric tops. The oblate type looks more like a 3-d picture of earth, while a prolate resembles an image of a football. The rotational transitions can be denoted as the quantum labels

$$J'k_a'k_c' \rightarrow J''k_a''k_c'' \tag{22}$$

where $k_a$, $k_c$ are projections of $J$.

## 1.3 Centrifugal Distortion

When rotating, molecules undergo a deformation causing them to be displaced from their equilibrium structure. When the molecule in Fig. 2 is excited by microwave radiation, it causes the molecule to rotate faster. This faster rotation causes the bond between $M_1$ and $M_2$ to be slightly stretched. In the case of a diatomic molecule, there is only one structural parameter which is the bond length. Because of this centrifugal effect, the bond length will be stretched a bit longer. As you can see from eq. 8, the moment of inertia will also increase. This causes the rotational constant (*B*) to become smaller, as you can see in eq. 12. Experimentally this will cause the frequency to be shifted lower in the rotational spectrum. In order to account for the shift, it is useful to understand the Hamiltonian operator corresponding to centrifugal distortion. The operator for that system is composed of

$$\widehat{H}_{CD} = -D\hat{J}^4 \tag{23}$$

where the D is the centrifugal distortion constant. The centrifugal distortion constant can be linked to the stretching vibrational frequency through eq. 24:

$$D = \frac{\hbar^4}{2h}\frac{m}{f(I_e)^3} = \frac{4B_e^3}{\omega_e^2} \tag{24}$$

where the $\omega_e = (\frac{1}{2\pi})(\frac{f}{m})^{\frac{1}{2}}$ denotes the vibrational frequency [60]. $B_e$ is the equilibrium rotational constant. The negative sign in front of *D* is to ensure the constant is positive. When we utilize the classical Hamiltonian operator for a semirigid nonvibrating molecule, which is composed of the energy of a rigid rotor and the energy of distortion, then we can reduce the classical Hamiltonian operator to $-\frac{1}{8}(\frac{\partial\mu}{\partial R})_e^2(\frac{1}{f})\hat{J}^4$. The $\hat{J}^4$ arises from the product of the distortion constants and the angular momentum. The *f* term is the force constant that arises from the potential energy, and R is the equilibrium bond length. When the partial derivative is evaluated, the term becomes eq. 24 [18,90]. Like eq. 15, eq. 25 accounts for the transition frequencies of a diatomic molecule undergoing centrifugal distortion.

$$\nu_{J\rightarrow J+1} = 2B(J+1) - 4D(J+1)^3 \tag{25}$$

The centrifugal distortion Hamiltonian for asymmetric tops is

$$\hat{H}_{CD} = \frac{\hbar^4}{4}\sum_{\alpha,\beta,\gamma\delta}\tau_{\alpha,\beta,\gamma\delta}\hat{J}_\alpha\hat{J}_\beta\hat{J}_\gamma\hat{J}_\delta \tag{26}$$

where $\tau_{\alpha\beta\gamma\delta}$ are the distortion constants and can be further explained in [18,90] and the α, β, γ, and δ = *a, b,* or *c.* The centrifugal distortion effects highly depend on the angular momentum operators and the $\tau_{\alpha\beta\gamma\delta}$ constants. Since the angular momentum operator $\hat{J}_\alpha$ has a non-commuting character, there will be eighty-one terms for the $\tau_{\alpha\beta\gamma\delta}$ constants. Fortunately, many of those terms are equivalent, and would further reduce the Hamiltonian to six groups of terms for the first-order expression. The new Hamiltonian would be described as

$$\hat{H}_{CD} = \frac{\hbar^4}{4}\sum_{\alpha,\beta}\tau_{\alpha,\alpha,\beta\beta}J_\alpha J_\beta \tag{27}$$

Where after a few coefficients are taken from Table 8.4 and 8.5 from Gordy *et al.*, the Hamiltonian can be diagonalized and plugged into the eq. 1 [90]. Producing the energy of centrifugal distortion for an asymmetric top, eq. 28.

$$E = -D_J J^4 - D_{JK} J^2 J_z^2 - D_k J_z^4 - \delta_J J^2 - \delta_K J_z^2 \tag{28}$$

The terms $D_J$, $D_{JK}$, $D_K$, $\delta_J$, and $\delta_K$ are the quartic centrifugal distortion constants for the Watson a-type [41].

## 1.4 Nuclear Quadrupole Coupling

When a molecule contains an atom or more with a nuclear spin of I = 1 or greater, the nuclear spin(s) will couple with the electric field surrounding the nucleus (nuclei) causing splittings in that rotational transition. Therefore, instead of one line being produced in the rotational spectrum, several lines will arise. This is called nuclear quadrupole coupling effect. Such interactions cannot happen when atoms with nuclear spins of 0 or ½ exist in the molecule because the quadrupole moments of those nuclei are spherically symmetric. The nuclear quadrupole hyperfine structure provides information on electronic structure and chemical bonds [90]. A good example of a linear molecule that has nuclear quadrupole hyperfine structure is $HC_5N$ [36]. Because N has an I = 1 there will be a triplet splitting for every rotational transition. In order to study these types of molecules, we must use the Hamiltonian corresponding to nuclear quadrupole coupling $\hat{H}_{NQC}$ from (2). The general $\hat{H}_{NQC}$ is composed of

$$\hat{H}_{NQC} = \frac{eQ_{q_J}}{2\hat{J}(2\hat{J}-1)I(2I-1)}[3(I\cdot\hat{J})^2 + \frac{3}{2}I\cdot\hat{J} - I^2\hat{J}^2] \tag{29}$$

Where the *I* is the nuclear spin and $\hat{J}$ is the angular momentum. When these two terms are coupled the resultant is *F* the total angular momentum quantum number. Because *F* is the vector sum of *I* and *J*, the product is $F^2 = \hat{J}^2 + 2I\cdot\hat{J} + I^2$. Similarly, when $I\cdot\hat{J} = \frac{1}{2}(F^2 - \hat{J}^2 - I^2)$,the eigenvalues of $I\cdot\hat{J}$ are $\frac{1}{2}\left[F(F+1) - \hat{J}(\hat{J}+1) - I(I+1)\right] = \frac{C}{2}$, and for $(I\cdot\hat{J})^2 = \frac{C^2}{4}$. Finally, we can substitute these terms into eq. 29, when $\hat{J}I^2 = \hat{J}(\hat{J}+1)I(I+1)$. We obtain the energy of the first-order nuclear quadrupole coupling energy for a diatomic system

$$E_{NQC} = -eQ_qY(J,I,F) \tag{30}$$

where $-eQ_q = -\chi$ and the *Y(J,I,F)* becomes

$$Y(J,I,F) = \frac{\frac{3}{4}C(C+1) - I(I+1)\hat{J}(\hat{J}+1)}{2(2J-1)(2J+3)I(2I-1)} \tag{31}$$

where C is composed of diagonal elements

$$C = F(F+1) - I(I+1) - \hat{J}(\hat{J}+1) \tag{32}$$

and $F$ is the total angular momentum not the $F(J)$, which is related to the rotational energy levels[18,90]. The total angular momentum takes on the values of

$$F = \hat{J} + I, \hat{J} + I - 1, \dots, \left|\hat{J} - I\right| \qquad (33)$$

In eq. 29 the $e$ is the charge of the proton, $Q$ is the quadrupole moment, $q_J$ is the electric field gradient of the nucleus, and $Y(J,I,F)$ is the Casimer function[60]. The electric field gradient is composed of

$$q_J = -\frac{Q^J}{(2J+3)} \qquad (34)$$

which in eq. 30 denotes the energy depending on the coupling of the nuclear spin to the electric field gradient, producing the nuclear quadrupole coupling constant $\chi$. Thus, the coupling scheme that was used for these whenever there is an atom with $I$ contributing to the rotational spectra,

$$F = I + \hat{J} \qquad (35)$$

By using this coupling scheme one obtains the quantum labels of

$$J''F'' \rightarrow J'F' \qquad (36)$$

from eq. 29, one can obtain the asymmetric top representation

$$\hat{H}_{NQC} = eQq_J \frac{2\hat{J}+3}{\hat{J}} Y(J,I,F) \qquad (37)$$

where $eQ=\chi$ which produces the electric field gradient for an asymmetric top to be

$$q_J = \frac{2}{(\hat{J}+1)(2\hat{J}+3)} \sum_{g=a,b,c} q_{gg} \langle \hat{J}_g^2 \rangle \qquad (38)$$

and

$$\langle \hat{J}_g^2 \rangle = \left(\hat{J}, K_{-1}, K_1 \middle| \hat{J}_g^2 \middle| \hat{J}, K_{-1}, K_1\right) \tag{39}$$

Where the *Y(J,I, F)* terms have been explained beforehand. Therefore, producing the quadrupole energy to be

$$E_{NQC} = \frac{1}{\hat{J}(\hat{J}+1)}\left\{\chi_{aa}\left[\hat{J}(\hat{J}+1) + E(\kappa) - (\kappa+1)\frac{\partial E(\kappa)}{\partial \kappa}\right] + 2\chi_{bb}\frac{\partial E(\kappa)}{\partial \kappa} + \chi_{cc}\left[\hat{J}(\hat{J}+1) - E(\kappa) + (\kappa-1)\frac{\partial E(\kappa)}{\partial \kappa}\right]\right\} Y(J, I, F) \tag{40}$$

[18,90]. For asymmetric tops like 1,1-diiodoethane that this thesis will focus on later, the quantum label will be

$$J'' k_a'' k_c'' F_1'' F'' \rightarrow J' k_a' k_c' F_1' F' \tag{41}$$

The main driving force behind the quantum numbers in eq. 41 is that there are two nuclei that are contributing to the rotational spectrum. This will be described in more detail in chapter four.

## 1.5 Nuclear Spin-Rotation

Nuclear spin-rotation is quite different from what we saw in the section above. It arises when the nuclear spin couples to the molecule's rotation causing a shift in the spectrum. This can be defined as

$$\hat{H}_{NSR} = -\hat{\mu} \cdot H \tag{42}$$

where $\hat{\mu}$ is defined as the dipole moment that can also be considered as the nuclear spin magnetic moment is the molecules rotation. *H* is the molecular field gradient produced by the molecule's rotation. The term $\hat{\mu}$ is defined as

$$\hat{\mu}_I = g_I \beta_I \boldsymbol{I} \tag{43}$$

where the $\beta_I$ is the nuclear magneton, $g_I$ is the g-factor (which is dimensionless) for the atom with a nuclear spin. Since $\hat{\mu}$ and $H$ have a weak interaction, sometimes within the rotational spectrum these terms can be neglected. Because the molecule is rotating very quickly compared to ***I***, the electric field becomes normal. This causes the $\hat{J}$ term to be taken out of the set producing

$$H_{eff} = \langle H_J \rangle \frac{\hat{J}}{|\hat{J}|} = \frac{\langle H_J \rangle \hat{J}}{\hat{J}(\hat{J}+1)^{\frac{1}{2}}} \qquad (44)$$

Which yields the first-order nuclear spin-rotation Hamiltonian expression

$$\widehat{H}_{NSR} = \frac{g_I \beta_I \langle H_J \rangle}{[\hat{J}(\hat{J}+1)]^{\frac{1}{2}}} I \cdot \hat{J} \qquad (45)$$

where the $I \cdot \hat{J}$ term has already been discussed beforehand, and the off-diagonal terms of $H$ can be dropped, leaving the diatomic Hamiltonian operator for nuclear spin-rotation to be

$$\widehat{H}_{NSR} = C_I I \cdot \hat{J} \qquad (45a)$$

Where the $C_I$ is

$$C_I = \frac{1}{\hat{J}(\hat{J}+1)} C_I\left(|\hat{J}||\hat{J}^2|\hat{J}\right) = C_I \frac{\hat{J}(\hat{J}+1)}{\hat{J}(\hat{J}+1)} = C_I \qquad (45b)$$

$C_I$ is used here because the molecule only has one axis, z-axis[18,90]. The energy expression would be

$$E_{NSR} = \frac{C_I}{2}[F(F+1) - I(I+1) - \hat{J}(\hat{J}+1) \qquad (46)$$

For asymmetrical tops, the Hamiltonian is expressed to be

$$\widehat{H}_{NSR} = C_{J_{K_a K_C}} I \cdot \hat{J} \qquad (47)$$

where the $I \cdot \hat{J}$ can be treated as before and eq. 47 can be expanded into

$$C_{J_{K_a K_C}} = \frac{1}{\hat{J}(\hat{J}+1)} \sum_{g=a,b,c} C_{gg} \langle \hat{J}_g^2 \rangle \qquad (48)$$

where $C_{gg}$ are the diagonal elements of the nuclear spin-rotation coupling [18,19,36]. Thus eq.48 can finally become

$$\hat{H}_{NSR} = C_{aa} I_a \hat{J}_a + C_{bb} I_b \hat{J}_b + C_{cc} I_c \hat{J}_c \qquad (49)$$

Where the $C_{i,j}$ (i, j = a, b, or c) are the nuclear spin-rotation coupling constants with respect to their *a, b, c* axis. Once plugged into eq. 1, it would yield the energy expression

$$E_{NSR} = \frac{1}{4J(J+1)} \left\{ C_{aa} \left[ \hat{J}\left(\hat{J}+1\right) + E(\kappa) - (\kappa+1) \frac{\partial E(\kappa)}{\partial \kappa} \right] + 2C_{bb} \frac{\partial E(\kappa)}{\partial \kappa} + C_{cc} \left[ \hat{J}\left(\hat{J}+1\right) - E(\kappa) + (\kappa-1) \frac{\partial E(\kappa)}{\partial \kappa} \right] \right\} [F(F+1) - I(I+1) - \hat{J}(\hat{J}+1) \qquad (49a)$$

It should be noted that these terms sometimes do not play a large role in the rotational spectrum.

# CHAPTER II

# INSTRUMENTAL

## 2.1 Introduction

Microwave (rotational) spectrum of ammonia was first recorded in 1934 [15]. Fig. 6. shows a commercial conventional waveguide microwave spectrometer manufactured in 1970s. This spectrometer is kept at room temperature and uses a klystron source. The klystron source bombards microwave radiation into the sample cell (wave guide), allowing the molecules to absorb radiation. The molecules absorption of radiation will then get picked up by a detector, and a readout is produced in the frequency domain.

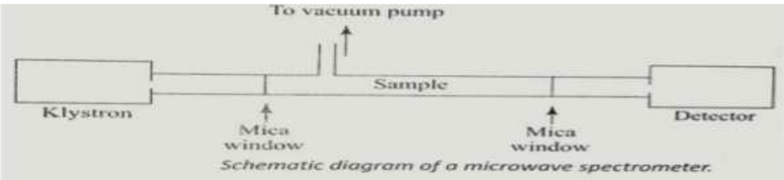

*Schematic diagram of a microwave spectrometer.*

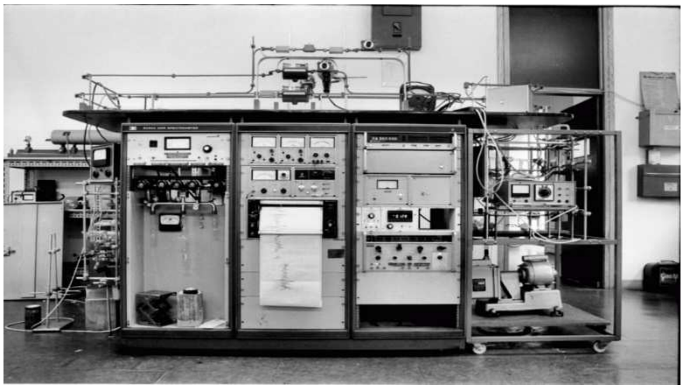

Figure 6. Shows the conventional waveguide (top) first commercial microwave spectrometer from HP (bottom) [105].

In early 1980, the cavity-based Fourier transform microwave (FTMW) spectrometer was invented by Flygare and Balle at the University of Illinois Urbana-Champaign and yielded a high resolution, high sensitivity microwave spectrometer [84]. The resonance frequency range is estimated to be about 1 MHz. In 2008, a chirped-pulse FTMW spectrometer was invented by Pate and coworkers at the University of Virginia [8,32]. This spectrometer keeps its high-resolution capabilities and probes a much larger frequency range than that of the cavity-based spectrometer. This section describes the two microwave spectrometers that were utilized throughout my master's thesis. Those two spectrometers can be seen in Fig. 7.

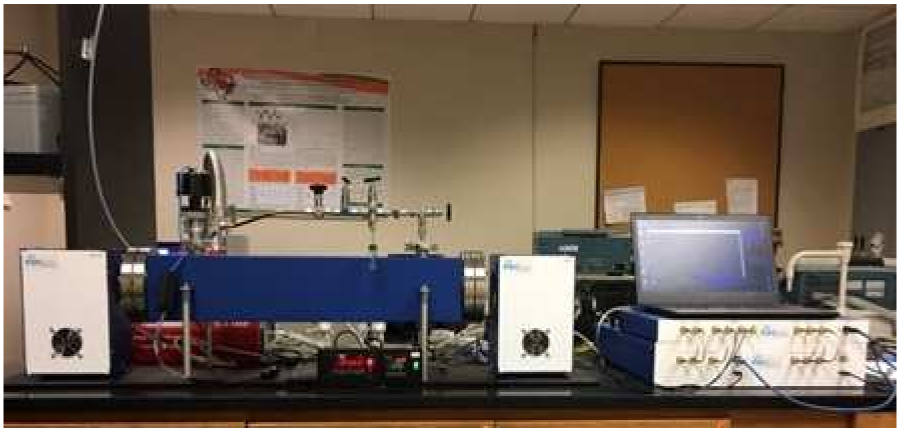

Figure 7. Shows the cavity-based FTMW spectrometer at NCTU (top) and the BrighSpec. chirped-pulse FTMW spectrometer at UTRGV (bottom).

The top of Fig. 7 shows the cavity-based FTMW spectrometer that was used in this project, which is housed in Professor Yasuki Endo's lab at the National Chiao Tung University in Hsinchu, Taiwan. The cavity-based FTMW spectrometer will be discussed in section 2.2, including the Fabry-Perot cavity, supersonic expansion, and cavity-based Fourier transform method [84]. The bottom of Fig. 7 shows the BrighSpec. Chirped-pulse FTMW spectrometer and is housed at the University of Texas Rio Grande Valley in Professor Wei Lin's laboratory.

## 2.2 Cavity-Based FTMW Spectrometer

### 2.2.1 Fabry-Perot Cavity

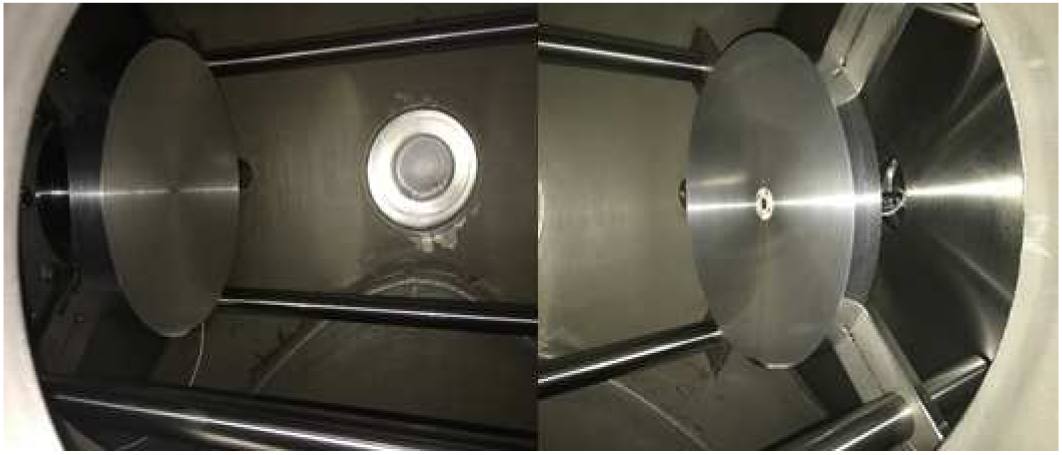

Figure 8. The left mirror is the tunable mirror that has the microwave antenna at the center. The right mirror injects the sample under supersonic expansion.

The Fabry-Perot cavity is housed in a stainless-steel chamber (top of Fig. 7) that is composed of two concave aluminum mirrors as shown in Fig. 8. In the spectrometer used for this study, one mirror has a microwave antenna at the center. This mirror is tunable. The other mirror injects the sample into the cavity and is fixed. In other cases, both mirrors have a microwave antenna. Where one antenna bombards microwave radiation, and the other receives molecular radiation (or so-called free induction decay). In our case, the tunable mirror will propagate microwave radiation and collect the molecule's radiation. Those two mirrors should be separated by a certain amount of distance. The importance of the distances is so that the two mirrors can create a resonant wave throughout the duration of the experiment. The mirrors will need to be tuned before the start of every new measurement. Because the sample slit is parallel to the microwave antenna, there will be a Doppler splitting (Fig. 9). Doppler splitting arises when microwave radiation is being propagated in between the two mirrors and onto the sample. When molecules emit radiation, it will flow in every direction. The molecular radiation that does flow in the direction of the antenna will get collected. The radiation that is not in that direction will just die out. After that antenna collects the first molecular radiation that hit it, the molecular radiation opposite to the antenna's direction arrives a little later and is collected. The reason the molecular radiation arrives later is that it traveled to the other mirror and was bounced back towards the microwave antenna. This signal is Fourier transformed from time-domain (left side of Fig. 9) to the frequency domain (right side of Fig. 9), which will appear in a doublet. The Doppler splitting will increase with the frequency. The reason behind this is that the higher the frequency means less time it takes for the Doppler to form.

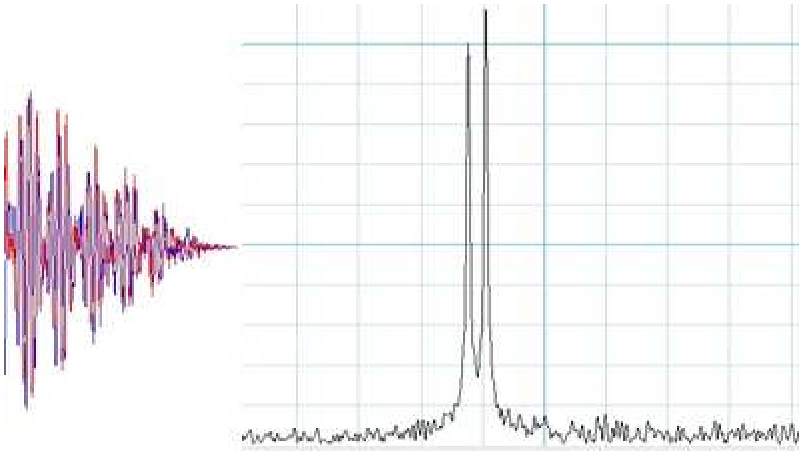

Figure 9. Shows the $2_{22}$-$1_{10}$ rotational transition of 1,1-diiodoethane with a Doppler splitting of 53.4 kHz. It also shows a spectrum in the time domain on the left and frequency domain on the right.

### 2.2.2 Supersonic Expansion

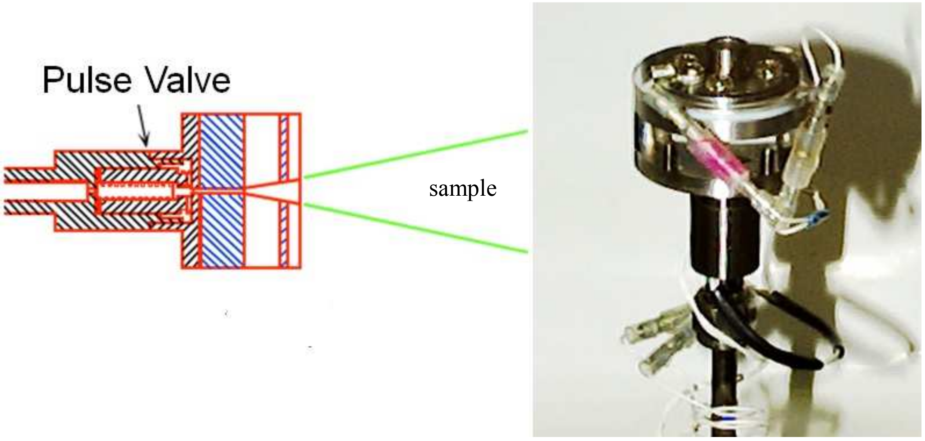

Figure 10. Shows the pulse nozzle injecting 1,1-diiodoethane [101]

When a sample in the gas-phase is injected and carried by an inert carrier gas (e.g. argon, neon, etc.) into the cavity, it is undergoing a change of pressure rapidly. This is because the sample is being pulsed through a narrow slit nozzle as seen in Fig. 10 (left side shows a schematic of the nozzle and the right side shows a picture of the nozzle) that is located at the center of the aluminum mirror (right side of Fig. 8). A diffusion pump is hosted under the stainless steel chamber. In order to pump to high vacuum, a mechanical pump is needed to pre-pump to $10^{-3}$ torr, then a diffusion pump is turned on to allow the pressure to be pumped to down

$10^{-7}$ torr. Once the sample is being pulsed in, the vacuum pressure is usually estimated to be $10^{-5}$ torr. The backing pressure is typically around 1 atm (760 torr). The process when molecules are flowing rapidly from room to vacuum pressure through a narrow slit is called supersonic expansion. The molecules will travel very uniformly through that slit and into the cavity, minimizing collision forces and allowing molecules to exist in their vibrational and rotational ground state. Furthermore, it allows the molecules to be at a rotational temperature of 10 K or below [84,12].

### 2.2.3 Cavity-Based Fourier Transform Method

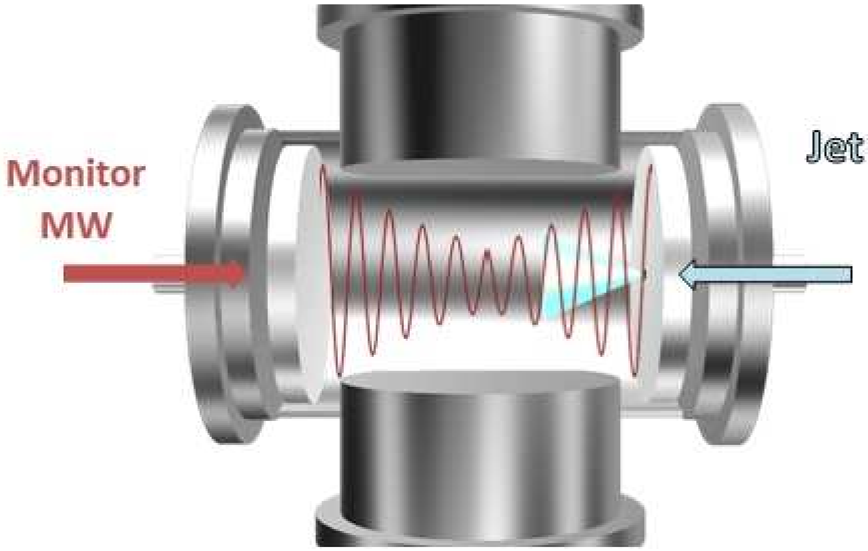

Figure 11. Demonstrates microwave radiation being propagated from the microwave antenna, while the sample is injected into the cavity [13].

This section will describe a detailed mechanism of how a cavity-based Fourier transform microwave spectrometer functions. First, the chamber must be pumped down to adequate vacuum pressure. Once that correct vacuum pressure has been achieved, a series of procedures are used to obtain a microwave spectrum of the sample. This can be seen in the pulse sequence scheme in Fig. 12. It demonstrates the timing of each pulse. First, the sample is pulsed in and stopped as shown on the rightside of Fig. 11. After a very short time, microwave radiation is pulsed in as seen on the left side of Fig. 11. Two possible scenarios can happen here, if the microwave radiation does not match the frequency of the molecule, then nothing happens. If the radiation does match the frequency of the molecule, it would interact with the molecule's dipole moment causing it to be promoted to its excited rotational level. After a short time, the microwave pulsing is stopped and those molecules in their excited rotational state will decay back to their ground state. While decay is undergoing, the molecules will release molecular radiation (as seen in the left side of Fig. 9). A trigger is used to tell the microwave antenna to collect the molecular radiation. Since the molecular radiation is weak, a microwave amplifier is used to boost the power signal. All this is collected in the time domain. Therefore, a Fourier transform is performed to obtain a frequency domain spectrum. The advantage of application of Fourier transform technique is that it will allow the spectroscopists to carry out thousands of measurements instead of one, then add them together. During this addition, the noise level will average to a much lower level while the intensity of the true lines stay the same. It significantly improves the signal to noise ratio of the instrument. Such process can be seen in the right side of Fig. 9.

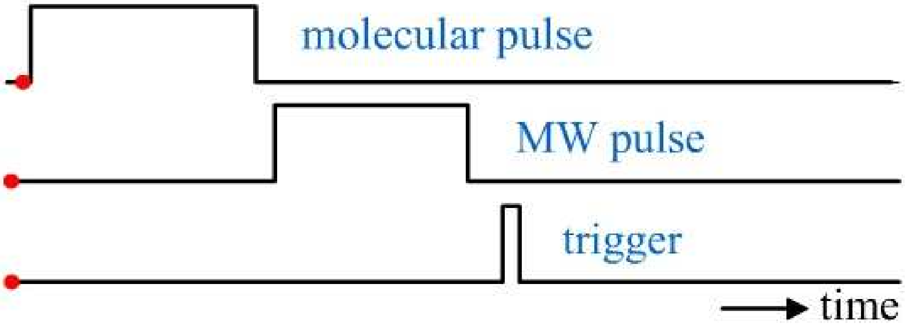

Figure 12. Shows the molecular pulse, microwave pulse, and trigger [94].

## 2.3 Chirped-Pulse FTMW Spectrometer

### 2.3.1 Differences of Cavity-Based and Chirped Pulse FTMW Spectrometers

In this section, I will describe the differences of cavity-based and chirped-pulse. Chirped-pulse FTMW spectrometer is quite similar to the cavity-based one in the sense that it still probes the rotational spectrum of gas-phase molecules. The difference is the design of the spectrometer. Unlike the cavity-based which is a narrowband technique, the chirped-pulse is a broadband technique. The chirped-pulse can scan a larger frequency region versus the cavity-based. For example, Prof. Endo's spectrometer has a scanning capacity of 1 MHz, whereas Prof. Pate's spectrometer has a scanning capacity of 10 GHz [8,32]. This is because the chirped pulse spectrometer utilizes a chirp-pulse microwave pulse generator to allow measurements of a large frequency range. In the cavity-based FTMW spectrometer the high resolution arises from the Fabry-Perot cavity. The bandwidth, however, is limited by the resonance frequency range of the cavity of about 1 MHz. In order to measure the same frequency range of 10 GHz in the chirped-pulse spectrometer, one would have to carry out 10,000 measurements in the cavity-based instrument. This is why the chirped-pulse FTMW spectrometer revolutionized the game. Instead of using the Fabry-Perot cavity, the chirped-pulse spectrometer uses the horn antennas inside the stainless steel chamber to propagate the microwave radiation as seen in Fig. 13.

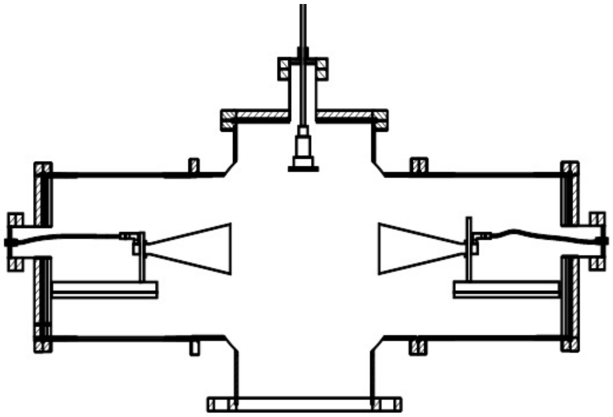

Figure 13. Shows the inside of the chamber of Prof. Pate's chirped-pulse FTMW spectrometer [8].

The chirped-pulse FTMW spectrometer works by generating a wide frequency range of microwave radiation, preamplified using a power amplifier, which is then transferred by cables onto a source horn antenna. This source horn antenna will propagate the microwave radiation into the vacuum chamber, and at the same time, the sample is being injected into the chamber and undergoing supersonic expansion. The microwave radiation will be broadcasted along a large frequency range, which will match all the molecule's intrinsic frequencies causing excitations to the next rotational levels. After a short time, the microwave radiation will be stopped and the molecular radiation is being released due to decay back to the ground state. Therefore, the molecular radiation will be collected by the receiving horn antenna. Where the molecular radiation is amplified and transferred through the cables onto a digital storage oscilloscope. Since all these data points are in the time domain, a Fourier transform is performed to obtain the data in the frequency domain.

### 2.3.2 BrightSpec. K-Band FTMW Spectrometer

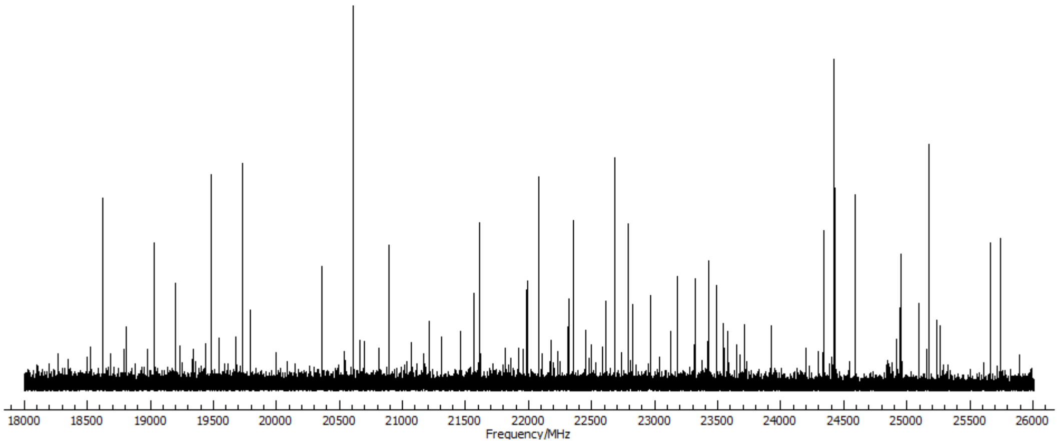

Figure 14. Shows the rotational spectrum of acetic acid at 300 K within 100,000 average shots from 18-26 GHz region produced from the Maria instrument.

This section is devoted to the K-band chirped-pulse FTMW spectrometer shown in Fig. 6. This instrument is a commercial product developed by BrightSpec. Inc, which was co-founded by Professor Brooks Pate. The spectrometer is different from the original chirped-pulse FTMW spectrometer. The reason is that it is a room temperature spectrometer, unlike the supersonic expansion process that other chirped-pulse spectrometers use. It can study the rotational spectrum of molecules in the room temperature which allows us to also study the vibrationally excited states of certain molecules or higher energy conformations. In our instrument, the horn antennas are outside, which is a benefit because it allows us to align the antennas without needing to break vacuum. In Fig. 6 (bottom), the left side of picture shows the mechanical section of the spectrometer. This includes the turbo pump, the stainless steel sample cell chamber along with the microwave horn antennas, and the sample manifold. The turbo pump is mounted at the back of the stainless steel chamber. It allows the pressure to be directly pumped down to $10^{-6}$ torr from room pressure. Once the turbo pump has pumped down to the required pressure, the molecules can be transferred into the sample cell given that the vapor pressure of the molecule is higher than a couple mtorrs. Once the pressure has stabilized, measurements can be taken. Another benefit of the stainless steel chamber is that it can be heated. This can potentially increase the population of the molecules to their excited vibrational states, allowing spectroscopists to study the rotational levels of vibrationally excited state. The sample manifold, which is mounted above the stainless steel chamber, allows us to control the amount of sample that will go into the chamber. Next are the microwave horn antennas, which are similar to the ones described beforehand. The right side of Fig. 6 is the electrical portion of the instrument. The first box on the top is the microwave synthesizer. Where the microwave radiation will be transferred through the cables into the source microwave horn antenna. From here the microwave radiation is propagated to the sample cell causing the molecules to be excited. Once that microwave radiation stops, the molecule will decay back to its ground state, releasing molecular radiation. The molecular radiation is propagated to the receiving horn antenna, where it is amplified and transferred through cables to the bottom box, the microwave detector. Here the molecular radiation is converted from the time domain into the frequency domain via Fourier transform. The bandwidth of this instrument is 18 MHz. The frequency ranges from 18-26 GHz as seen in Fig. 14. Accordingly it will take the instrument 445 measurements to scan the whole frequency range. The fact that this instrument runs with the sample molecule static in the cell, the pump can work at almost 100% duty cycle, whereas in the instruments with pulsed jet it is limited to about 10 Hz (or 0.02% duty cycle) due to sample injection. This significantly improved pumping rate plus the benefit of using a custom digitizer with essentially no resetting time between acquisitions allows much larger number of measurements to be taken for each step. The maximum averaging cycles is 16 millions for this instrument, significantly improves its sensitivity. The typical number of averaging cycles we use for this instrument is 100 k. Using the number, it takes about 20 minutes to finish scanning the full 8 GHz range of the spectrometer.

Since this is the first time the spectrometer is introduced in the literature, I will include the operation procedure in Appendix A.

## CHAPTER III

## THEORETICAL CALCULATIONS

### 3.1 Methods

As seen in eq. 1 from Chapter 1, the time-independent Schrödinger's equation is utilized for obtaining energies and chemical or molecular properties. Generally, an equation like eq. 1 is composed of a mathematical operator ($\hat{O}$) that is applied onto a wavefunction (ψ), which produces an eigenvalue ($c$) that is multiplied by the same eigenfunction (ψ). This can be seen in a generic equation shown below.

$$\hat{O}\psi = c\psi \tag{50}$$

If we allow the $\hat{O} = \hat{H}$ and $c = E,$ while $\psi$ is a continues function, then we obtain the time-independent Schrödinger's equation from Chapter 1. Because the molecular system of study is undergoing rotation which is a real time property, it would behoove us to understand the time-dependent Schrödinger equation as well. Eq. 51 shows the time-dependent Schrödinger equation

$$\hat{H}\psi(x,t) = i\hbar\frac{\partial\psi}{\partial t} \tag{51}$$

where $\hat{H}$ does not contain information on time [21]. Thus, we introduce eq. 52 as an Ansatz, an approach that simplifies the problem at hand. The Ansatz allows us to separate variables for the time-dependent Schrödinger equation, where we obtain a wavefunction like

$$\psi(x,t) = \psi(x)f(t) \tag{52}$$

If we plug in eq. 52 into eq. 51, and divide both sides by $\psi(x)f(t)$, we would obtain

$$\frac{\hat{H}\psi(x)}{\psi(x)} = \frac{i\hbar df}{f(t)dt} \tag{53}$$

and since $\hat{H}$ does not contain any property of time, the left hand side can only depend on *x*, while the right hand side can depend on *t* time. Therefore, both sides of the equation will produce a constant [21]. If we let the constant be *E*, then we obtain

$$\hat{H}\psi(x) = E\psi(x) \tag{54}$$

The Schrödinger's equation and

$$\frac{df}{dt} = \frac{-i}{\hbar}Ef(t) \tag{55}$$

Where eq. 55 can be integrated into

$$f(t) = e^{\frac{-iEt}{\hbar}} \tag{56}$$

And the $\psi(x,t)$ takes on the form of $\psi(x)e^{\frac{-iEt}{\hbar}}$. Since the terms from the statement before hand are independent of time, the $\psi(x)$ can be called a stationary state [21]. The stationary states are of importance to spectroscopists and hold dynamic information of that system.

The time-independent Schrödinger's equation of a molecular system (from eq. 1) contains information on the kinetic energy of the electrons and the nuclei of the atoms. The molecular Hamiltonian operator is composed of

$$\hat{H} = -\sum_{i}^{electrons}\frac{\hbar^2}{2m_e}\nabla_i^2 - \sum_{A}^{nuclei}\frac{\hbar^2}{2m_A}\nabla_A^2 - \sum_{i}^{electrons}\sum_{A}^{nuclei}\frac{e^2 Z_A}{4\pi\varepsilon_0 r_{iA}} + \sum_{i>j}^{electrons}\frac{e^2}{4\pi\varepsilon_0 r_{ij}} + \sum_{A>B}^{nuclei}\frac{e^2 Z_A Z_B}{4\pi\varepsilon_0 R_{AB}} \tag{57}$$

where the first two terms are the kinetic energy of the electrons and the nuclei. The third term is the potential energy due to electron-nuclei attraction. The fourth term is the potential energy due to electron-electron repulsion, and the fifth term is the potential energy of the nuclear-nuclear repulsion. Since the nuclei of atoms are much heavier, they can be held stationary. This causes the nuclear coordinates to be frozen and contribute nothing to the Hamiltonian operator. By doing this, we can negate the second term and add the fifth term after we have acquired the energy of the system. The electrons, on the other hand, are much lighter and can move much quicker [46]. This assumption is also known to be the Born-Oppenheimer approximation [46]. The $r_{ln}$ represents the distance between $l$ and $n$, $i$ is the subscript for electrons, A is for nuclei, $m_e$ and $m_A$ are the masses of the electron and nucleon, respectively. Thus, we need to only focus on solving the energy that depends on the set of atomic coordinates. If we allow $\hbar = 1$, $m$=1, $e$ =1, and $k_0=4\pi\varepsilon_o=1$, then eq. 57 can become

$$\hat{H} = \sum_{i}^{electrons} -\frac{\nabla_i^2}{2} + \sum_{i}^{electrons}\sum_{A}^{nuclei}\frac{-Z_A}{r_{iA}} + \sum_{i>j}^{electrons}\frac{1}{r_{ij}} \tag{58}$$

reduced to atomic units. 1 atomic unit is also known to be 1 Hartree = 2625.5 kJ/mol [21]. Eq. 58 is also known to be the electronic Hamiltonian. When plugged into the Schrödinger's equation, we obtain

$$\left(\sum_{i}^{electrons} -\frac{\nabla_i^2}{2} + \sum_{i}^{electrons}\sum_{A}^{nuclei}\frac{-Z_A}{r_{iA}} + \sum_{i>j}^{electrons}\frac{1}{r_{ij}}\right)\Psi\overrightarrow{(r_r)} = E_{el}\Psi\overrightarrow{(r_r)} \tag{59}$$

where the eigenvalue of the Hamiltonian operator is the electronic energy $E_{el}$. The $E_{el}$ is the energy that arises from the movement of electrons along with the electrostatic energies of all comparable particles (formally defined as a potential energy surface). This is still considering that the nuclei remain fixed. The wavefunction, on the other hand, must take into consideration the electron spin. Once that electron spin is considered, there must be another electron spin to counter that spin, as denoted in the Pauli exclusion principle. Therefore, the wavefunction that is utilized is

$$\Psi(\overrightarrow{r_1},\overrightarrow{r_2}) = -\Psi(\overrightarrow{r_2},\overrightarrow{r_1}) \tag{60}$$

where it must consider the antisymmetric exchange of the two particles. Basically, in quantum chemistry, there are several fundamental postulates that these equations must conform too. Although it is not my intention to describe them in this thesis, they are important in understanding all quantum mechanical (chemical) systems and can be found in ref. [21,46,19]. In this section, I will be describing *ab initio* and quantum chemical calculations along with basis set.

### 3.2 *Ab initio* Calculations

*Ab initio* means "from the beginning". Therefore, it is a useful method to take into consideration when starting to understand molecules in their initial form. The first *ab initio* method that was the "go-to" method was utilized for many years in quantum chemistry was the Hartree-Fock method [25,89]. Many years later the second-order Møller-Plesset perturbation theory popped up and produced better results than its predecessor [20]. Lastly is coupled-cluster single double theory, which predicts the best results at the moment. Although some methods were not utilized for the current study, I would still like to discuss them, as they are all important in understanding quantum chemistry.

### 3.3 Hartree-Fock Method

The Hartree-Fock (HF) method first came out in 1928 shortly after Schrödinger's equation was formulated [25,89]. HF uses an effective one-electron Hamiltonian for each electron in the system that has an effective potential that is determined by a mean-field approximation. In addition to the attraction of the electron to the nuclei, each electron will interact with and be repelled by a field that arises from the average charge distribution that is generated by the other electrons in their orbitals. We can denote this type of interaction as Coulombic type interactions, which exist between electrons of a given spin as well as those of other spins. Another type is purely quantum mechanical and arises from the antisymmetry of the electronic wavefunction, which is also indistinguishable [46,19,25,89]. The latter interactions only exist between electrons of the same spin and are called exchange interactions [21,46,19,25,89]. The remaining effects are neglected by the HF wavefunction because they rely on given interactions between pairs of electrons, irrespective of their spins. This falls under the category of correlation, which MP2 and CCSD can achieve [21,46,19,25,89]. A generic restricted HF wavefunction with even number of electrons is comprised of

$$\Psi(r) = \frac{1}{\sqrt{N!}}\left(\begin{vmatrix} \phi_1\alpha(1) & \phi_1\beta(1) & \cdots & \phi_{\frac{N}{2}}\beta(N) \\ \phi_1\alpha(2) & \cdots & & \\ \cdots & \cdots & & \cdots \\ \phi_{\frac{N}{2}}\alpha(N) & \cdots & \cdots & \phi_{\frac{N}{2}}\beta(N) \end{vmatrix}\right) \tag{61}$$

which shows the molecular orbital subscript to range from 1 to *N/2*, while the spatial part ranges from 1 to *N*. Each molecular orbital will appear twice for a given electron. Therefore, there will be as many columns and rows as there are electrons in the system. The electron spin function $\alpha(\omega)$ and $\beta(\omega)$ can range from 1 to *N*. Because orbitals are doubly filled, the spatial part can appear twice in the determinant. Thus, giving the same amount of parameters in the determinant as there are electrons in the system. Because there are *N*/2 spatial parts, the orbitals available will be occupied by the electron $\omega$ as seen below

$$\Phi_{2i-1} = \phi_i(\overrightarrow{r_1})\alpha(\omega) \qquad i = 1,2,3 \ldots N/2 \qquad (62)$$

$$\Phi_{2i} = \phi_i(\overrightarrow{r_1})\beta(\omega) \qquad i = 1,2,3 \ldots N/2 \qquad (63)$$

Thus, the total wavefunction is the sum of the products of spin orbitals. Furthermore, it is the sum of Hartree products like $\phi_1\alpha(1), \phi_1\beta(2), \phi_2\alpha(3), \phi_2\beta(4) \ldots \phi_{\frac{N}{2}}\alpha(N-1), \phi_{\frac{N}{2}}\beta(N)$ [31]. In eq. 62 and 63, the $\alpha$ term would yield odd numbers and the $\beta$ term would yield even spin terms. Another way to see eq. 61 is as a Slater determinant. It considers the antisymmetric property of the electrons as shown in eq. 60. When plugged into eq. 1, the HF wavefunction can be in the form of a Slater determinant, and allow the energy of the system to be given by

$$E_{el} = \langle\psi|\hat{H}_{el}|\psi\rangle \qquad (64)$$

where variational theorem can be applied, which would overshoot the energy to its true value. This would allow a better approximation for the wavefunction and minimize the energies within that functional [14]. The molecular orbitals that are produces can be integrated as a set linear combination of atomic orbitals. Another way to see the HF method is by the Self-consistent field method. This method considers an approximate Hamiltonian that solves the Schrödinger equation, and obtains an accurate set of molecular orbitals. Those approximate and accurate orbitals are then plugged into the Schrödinger equation again. They continue this process until they reach convergence [14]. HF is a good method for a starting point of any project. In order to obtain better results, one must employ a higher level of *ab initio* methods.

### 3.4 Basis Set

The basis set is a collection of mathematical functions that are used to build the electronic wavefunction for a system of study. By using a basis set the electron is restricted to a certain region of space. Thus, by using a higher-level basis set, we can allow fewer restraints on the electrons, allowing more accurate approximations to be obtained. A primitive is a basis function, which is a composition of a linear combination of several Gaussian functions assigned to atomic orbitals of each atom in the molecule of study. There are several kinds of basis sets, like split-valence, polarized, and diffuse functions. Where the split-valence basis set will treat valence orbitals as a linear combination of Gaussian primitives with a more complex structure that just a summation. In the case of polarized basis set, it allows the orbital to change shape by adding angular momentum to those orbitals. For diffuse functions, they allow the orbitals of s- and p-type to occupy a bigger volume of space. Anytime a diffuse function is added it is taking into consideration the electrons that are far away from their nuclei. This is a good basis set for molecules with high electronegativity, lone pairs, an anion, cation, excited states, etc. These basis sets can be combined in order to improve the functional. For instance, the basis set that was utilized in this master thesis was the aug-cc-pVTZ, which was invented by Dunning and coworkers [81]. In this basis set, the cc-pVTZ is the parent basis functional that includes polarization functions. The VTZ is considering the split-valence triple zeta correlation, in which triple zeta contains a total of 30 basis functions.There are other types that can be described in the Gaussian book [31].

### 3.5 Second-Order Møller-Plesset Perturbation Theory

The second-order Møller-Plesset (MP2) perturbation theory first came to be in 1934 and is an improvement of the HF method and is an approach to trying to solve the electron correlation problem. It applies the Rayleigh-Schrödinger perturbation theory to the Hamiltonian in order to account for the electron correlation [25,89,20]. Generally, this approach uses an approximation on a problem that already has a known solution, and perturbs it. In this case it takes the HF wavefunction/energy and then applies perturbation to it. It will then produce approximate solutions to the real problem in terms of the exact solutions to the zeroth-order problem. The MP2 theory will split the Hamiltonian into two parts as shown in eq. 65

$$\widehat{H}_{MP} = \widehat{H}_0 + \lambda\widehat{V} \tag{65}$$

where the $\widehat{V}$ is the small perturbation to the Hamiltonian, λ is a dimensionless parameter, and $\widehat{H}_o$ is denoted to be

$$\widehat{H}_0 = \sum \widehat{F}_V \tag{66}$$

which shows the summation of the Fock operator in the unperturbed problem [4-6]. When we introduce λ, the energy and wavefunction become dependent on the λ term. Since this becomes unsolvable in a way, we apply Taylor series expansion to account for the perturbation. By expanding the exact wavefunction along with its energy, the HF wavefunction and energy produce

$$E = E^{(0)} + \lambda E^{(1)} + \lambda^2 E^{(2)} + \cdots \tag{67}$$

along with the HF wavefunction which is

$$\psi = \psi_0 + \lambda\psi^{(1)} + \lambda^2\psi^{(2)} + \cdots \tag{68}$$

Where we substitute eq. 67 and eq. 68 into the Schrödinger’s equation we can obtain,

$$\widehat{H}_0\psi_0 = E^{(0)}\psi_0 \tag{69}$$

$$E^{(0)} = \langle\psi_0|\widehat{H}_0|\psi_0\rangle = \sum_i \varepsilon_i \tag{70}$$

the *n*th-order (MP*n*) energy [20,14,31]. Where in eq. 70, the energy is not the HF energy, but the sum of the orbital energies. When we utilize the first-order perturbation, we obtain the first-order energy expression

$$E^{(1)} = \langle\psi_0|\hat{V}|\psi_0\rangle \text{ and } \quad E^{(HF)} = E^{(0)} + E^{(1)} \tag{70a}$$

Which yields the HF energy. We can then take the HF energy and express the correlation energy to be the first term that is considered in eq. 71 [14]. The energy for a second-order perturbation theory is

$$E^{(2)} = E^{HF} - \sum_{s=0} \frac{|\langle\Psi_0|\hat{V}|\Psi_s\rangle|^2}{E_s - E_0} = E^{HF} - \frac{1}{4}\sum_{ijab} \frac{|\langle ij|ab\rangle|^2}{\varepsilon_a + \varepsilon_b - \varepsilon_i - \varepsilon_j} \tag{71}$$

where the single excitation term is 0 due to Brillouin's theorem, and the variationality of the wavefunction means that mixing in singles will not change the energy. The inclusion of triples, quadruples, etc. would not contribute because the Hamiltonian only contains one- and two-electron operators.  Eq.71 shows its only obtaining the double excitation [31]. The terms *i, j* are occupation terms that couple the electrons together, while *a* and *b* virtual terms. For triples, we would utilize the third-order perturbation expression, which is made up of

$$E^{(3)} = E^{(2)} + \sum_{st} \frac{\langle\Psi_0|\hat{V}|\Psi_s\rangle\langle\Psi_s|\hat{V}|\Psi_t\rangle\langle\Psi_t|\hat{V}|\Psi_o\rangle}{(E_s - E_0)(E_t - E_0)} \tag{71a}$$

where the *s* and *t* go over the double excitations and can range from single, double, triple, etc. [31]. Single, doubles, and triples are wavefunctions that are constructed by taking the HF wavefunction and replacing the specified number of occupied orbitals with the previous unoccupied orbitals.  Because eq. 71a does not include triples contribution,there is no way to obtain triples in three applications of $\hat{V}$. Therefore, it is crucial to include quadruples and go up to MP4 energies like below

$$E^{(4)} = E^{(3)} + \sum_{s,t,u} \frac{\langle\Psi_0|\hat{V}|\Psi_s\rangle\langle\Psi_s|\hat{V}|\Psi_t\rangle\langle\Psi_t|\hat{V}|\Psi_u\rangle\langle\Psi_u|\hat{V}|\Psi_o\rangle}{(E_s-E_0)(E_t-E_0)(E_u-E_0)} \tag{71b}$$

where the *s* and *u* will run over the doubles excitation, and *t* will cover singles doubles, triples, and quadruples excitation [31]. The MP2 perturbation theory is less expensive in terms of computational time than that of higher-level calculations. It provides a better approximation then that of the HF approximation method. A single point calculation at the MP2 level was utilized to predict the nuclear quadrupole coupling, nuclear spin-rotation, and other spectroscopic constants. For the purpose of this thesis, I will only delve into the second-order perturbation theory.

### 3.6 Coupled-Cluster Theory

The coupled-cluster theory is the "golden ticket" of calculations and was created in 1978 [67]. It provides the best computational results but is quite computationally expensive. Its full name is coupled-cluster theory with single and double excitation (CCSD). This method uses a cluster operator ($\hat{T}$) to construct a multi-determinant wavefunction that expands in a Taylor series format. The wavefunction is the product of the exponential cluster operator and the HF wavefunction as seen in eq. 72

$$\Psi = e^{\hat{T}}\Psi_{HF} = (1 + \hat{T} + \frac{\hat{T}^2}{2!} + \frac{\hat{T}^3}{3!} + \cdots)\Psi_{HF} \tag{72}$$

where the cluster operator takes on the form of

$$\hat{T} = \hat{T}_1 + \hat{T}_2 + \hat{T}_3 + \cdots + \hat{T}_n \tag{73}$$

and will end its expansion at *n*, since there are no further excitations after *n* [19]. For instance, if *n=2*,

$$\hat{T}_2 = \sum_{i<j}^{Occ} \sum_{a<b}^{Virt} t_{ij}^{ab}\ \psi_{ij}^{ab} \tag{74}$$

then the cluster operator takes on the doubles term, where the *t* term is noted to be the amplitude and is determined through the satisfaction of eq. 72 [19]. When eq. 72 is plugged into eq. 1, then

$$e^{\widehat{-T}}\hat{H}e^{\hat{T}}\Psi_{HF} = E\Psi_{HF} \tag{75}$$

we obtain the energy of the system. If we consider,

$$\Psi_{CCD} = e^{\hat{T}_2}\Psi_{HF} \tag{75a}$$

then the wavefunction is the coupled cluster-doubles excitation. Which when plugged into eq. 1 will produce the coupled-cluster doubles energy ($E_{CCD}$) [14]. When including triplet excitation, the cluster operator will range from

$$\hat{T} = \hat{T} + \hat{T}_2 + \hat{T}_3 \tag{76}$$

and will be known as coupled-cluster singles, doubles, and triples CCSD(T) theory. The CCSD(T) method takes into consideration the triple excitation determinant. When this cluster operator is plugged into eq. 1, then we obtain the CCSD(T) energy to be

$$E_{CCSD(T)} = E_{CCSD} - \frac{1}{36}\sum\nolimits_{\varepsilon}\frac{\left|\boldsymbol{u}_{ijk}^{abc}\right|^2}{\varepsilon_a+\varepsilon_b+\varepsilon_c-\varepsilon_i-\varepsilon_j-\varepsilon_k} \tag{77}$$

which includes perturbation theory and keeps all the important energies contribution that comes from the triple excitations. The term $\boldsymbol{u}_{ijk}^{abc}$ is a six-way matrix element of the Hamiltonian between the CCSD single and double excitation amplitudes along with the triple excitation term [31]. The other small downplay of this calculation is that it must be utilized with a large basis set [31]. Applying a larger basis set will help with more details from the chemical system. Although for our study, we utilized this type of calculation to predict the best structure of the molecule, which produces the best rotational constants.

### 3.7 Quantum Chemical Calculations and Texas Advanced Computing Center

There are many quantum chemical programs that have been created to better understand chemical and molecular systems. However, in this study only Gaussian 16 and Molpro were utilized [31,51]. Where Gaussian 16 "provides state-of-the-art capabilities for electronic structure modeling" [31], and Molpro "is a comprehensive system of *ab initio* programs for advanced molecular electronic structure calculations" [51]. The use of the Lonestar 5 and Stampede cluster computers housed at the Texas Advanced Computing Center (TACC) at the University of Texas Austin was utilized for computational calculations. I would like to thank TACC for their services as they were extremely helpful. Without these cluster computers no calculation would have been made possible [80].

# CHAPTER IV

# RESULTS

## 4.1 Understanding Alkyl Halides

Alkyl halides are cousins of hydrocarbons that are composed of F, Cl, Br, or I instead of hydrogen. They are important because of their use in industry and commercial production as fire retardants, extinguishers, organic solvents, and refrigerants [4,9,57,16,52,76,27,1,82,43,65]. In which they leech into the environment, drinking water, and atmosphere [62,48,61,87,100,64,78]. Because these alkyl halides are photochemically active, they will undergo photodissociation in the stratosphere where they produce a halogen anion. The anionic halogen will then react with the oxygen in ozone, causing the production of ClO, BrO, and IO radicals, which regenerate the halide and deplete the ozone layer further [95,102,63,68,49,47,73,55,54]. The main contributor of that depletion in the Antarctic region is a series of compounds called chlorofluorocarbons (CFC) which consist of trichlorofluoromethane, trichlorotrifluoroethane, dichlorotetrafluoroethane, and dichlorodifluoromethane [26]. These compounds have been reported to have long lifespans in the atmosphere, for example dichlorodifluoromethane can exist for up to190 years [83]. The Montreal protocol was passed in 1987. The purpose of this protocol was to stop the production of CFC's [88]. It dramatically reduced the concentration of these chemicals in the atmosphere. A study performed in China showed the decline in the production and consumption of CFC's in 1999 [45]. Although the battle between CFC's showed a good outcome there, other deleterious chemicals began to flow into the atmosphere, hydrochlorofluorocarbons (HCFC) and hydrofluorocarbons (HFC) [37]. In 2016 the Montreal protocol was amended to phase out these HFC and HCFC's [37,58]. Other important compounds that are sources for reactive halides in the atmosphere are the methyl halides ($CH_3X$; X= Cl, Br, or I). According to the World Meteorological Organization, chloromethane ($CH_3Cl$) is the most abundant source of chlorine in the atmosphere [97]. Bromomethane ($CH_3Br$) and iodomethane ($CH_3I$) are also the main precursor for bromine and iodine in the atmosphere. They come from the ocean, which is the natural source of bromomethane and iodomethane [98]. Iodomethane is more reactive than any other methyl halide [34]. It has been well studied that the conventional treatment of raw water by disinfection of chlorine, produces more carcinogenic alkyl halides [56]. Furthermore, they cause extreme deterioration to the soil that grows crops [86]. Therefore, it is imperative to study the structure these alkyl halides in the gas-phase, as they are ubiquitous. Microwave spectroscopy is a good technique to study the structure of these molecules. It helps us obtain a better understanding of the different conformations these molecules can have in the gas-phase. Halogen atoms have a nuclear spin. These nuclear spins contribute to additional splitting/shifting of the rotational transition, which have coined the term hyperfine splitting.

Previous studies performed by Gordy and coworkers on microwave measurements of the monosubstituted methyl halides, such as $CH_3{}^{35}Cl$, $CH_3{}^{79}Br$, $CH_3{}^{81}Br$, and $CH_3I$ have provided a better understanding on the bond lengths of C-X (X= Cl, Br, or I) and bond angles between <H-C-H [91]. They were not able to determine the bond angles of H-C-H very accurately for the methyl halides. This was because they could not determine $I_A$ as well as they determined $I_B$. Furthermore, the investigation was expanded to the deuterated methyl halides, such as $CD_3Cl$, $CD_3Br$, and $CD_3I$ where they found that because of the deuterated substitution they could not obtain enough information on the C-H displacement due to the zero-point vibrational energies [44]. In this study they did determine the nuclear quadrupole coupling constants that were in

agreement with what Gordy *et al.* observed [91]. They also state that their values for nuclear quadrupole constants were lower than those of the normal methyl halides [44]. This is due to the increased mass on the methyl group causing the potential energy to rise because of the bond between Cl-C is changes. It was not until Miller and coworkers reinvestigated the structure of deuterated methyl halides and normal methyl halides that they were able to obtain a better structural parameter for these species [77]. They determined better bond angles along <H-C-H as shown in Table 2.

| **Molecule** | **C-X (Å)** | **C-H or C-D (Å)** | **H-C-H (angle)** |
|---|---|---|---|
| **$CH_3Cl$** | 1.7810 | 1.113 | 110°31’ |
| **$CD_3Cl$** | 1.7810 | 1.104 | 110°43’ |
| **$CH_3Br$** | 1.9391 | 1.113 | 111°14’ |
| **$CD_3Br$** | 1.9391 | 1.104 | 111°26’ |
| **$CH_3I$** | 2.1392 | 1.113 | 111°35’ |
| **$CD_3I$** | 2.1392 | 1.104 | 111°37’ |

Table 2. Shows the bond length and bond angles of the methyl and deuterated halides.

Although the rotational constant *B* was determined very nicely, they could not report them with a large accuracy. Years later, several groups reinvestigated the $CH_3Cl$ and its isotopomers by using the high-resolution maser technique and molecular beam technique, in which they determined the rotational constant *B,* with great accuracy along with its nuclear quadrupole coupling constants, and the nuclear spin-rotation constants of $^{35}Cl$ and $^{37}Cl$ [74,2]. A similar study was performed on the ground state of $CH_3{}^{79}Br$ and $CH_3{}^{81}Br$, where they were able to determine the *B* rotational constant along with the quartic and higher order sextic centrifugal distortion constants. Furthermore, they determined the nuclear quadrupole coupling and the spin-rotation constants of both isotopomers, $^{79}$Br and $^{81}$Br [38]. For the case of $CH_3I$ a study performed by Boucher *et al.*, determined the structure and nuclear hyperfine components along with the centrifugal distortion constants (quartic and sextic) [22]. However, in the methyl chloride and bromide systems the higher order centrifugal distortion constant $H_{KJ}$ was not determined because of the inaccuracies. In the methyl iodide system, it was made possible through double resonance, where they helped the assignment. Young and Kukolich at al. were able to determine the J=1←0, K=0, J=2←1, K=0, J= 2←1, K=1 of $CH_3I$ and its deuterated species, where they were able to get a good understanding of the nuclear quadrupole coupling constants of both species [75].

Other set of molecular systems that are equally as important are the ethyl halides. The first of this series that came out when the halomethanes were first studied is, 1-chloroethane. Where the extra methyl group brings in another phenomenon, internal rotation. This will be discussed in the further section but is as equally as important as the nuclear quadrupole coupling constants. A complete structure analysis was performed on 1-chloroethane, where the *A* and *B* rotational constant were determined for 4 conformations [71]. They were not able to determine the *B* rotational constant to a certain degree because they were not able to determine a good value on the C-H bond length. However, they did determine that the equilibrium geometry is in the staggered conformation for all 4 conformations and is in excellent agreement from the structural parameters that were observed in methyl chloride system [77,74,71]. They also only determined the eqQ to be along the C-Cl bond [71]. In the reinvestigation of this molecule by Schwendeman *et al.*, they were able to obtain a more information and complete structural parameters and coordinates of every atom by using the Kraitchman's method [66,42]. Furthermore, they obtained the $\chi_{aa}$, $\chi_{bb}$, $\chi_{cc}$, and $\chi_{ab}$ which coincide with what had been found earlier [66]. Wagner *et al.* continued the study on $C_2H_5{}^{79}Br$ and $C_2H_5{}^{81}Br$, and determined the *B* and *C* rotational constants, structural parameters that were consistent with what was observed in Table 2, and the with the nuclear quadrupole diagonal terms [72]. They were not able to assign a few transitions even when they utilized second-order quadrupole effects [72]. The strong nuclear magnetic moment from the Br nucleus is the reason they observed so many splittings. It relates to the degree that was observed from the halomethanes systems. Flanagan *et al.* restudied 1-bromoethane system and determined the structure of 10 isotopic species by using the Kraitchman's substitution and better value of $\chi_{aa}$ and $\chi_{ab}$ nuclear quadrupole coupling constant [42,17]. The rotational spectrum of 1-iodoethane was first determined by Oka *et al.*, where they were able to assign the rotational constants, dipole moments, and the diagonal and off-diagonal term $\chi_{ab}$ [85]. They also determined the complete structure of the molecule and compared them to the to their ethyl halides as seen in Table 3.

| **Structure parameters** | **$C_2H_5Cl$** | **$C_2H_5Br$** | **$C_2H_5I$** |
|---|---|---|---|
| **$R_{C\text{-}X}$ (Å)** | 1.779 | 1.940 | 2.139 |
| **$R_{C\text{-}C}$ (Å)** | 1.550 | 1.550 | 1.540 |
| **$A_{C\text{-}C\text{-}X}$ (angle)** | 110°30’ | 110°30’ | 112°10’ |
| **$R_{C\text{-}H}$ (Å)** | 1.101 | 1.11 | 1.11 |
| **$A_{H\text{-}C\text{-}H}$ (angle)** | 110°00’ | 110°00’ | 110°00’ |

Table 3. Shows the bond length (R) and bond angle (A) for the different ethyl halides that have been previously mentioned.

Gripp *et al.* took another crack at the 1-iodoethane molecular system using high-resolution FTMW spectroscopy technique [39]. As mentioned before, the higher the resolution, the better the rotational spectrum and determination of smaller lines that are not seen in the conventional room-temperature technique. Where they were able to obtain a better understanding of the three diagonal nuclear spin-rotation and quadrupole coupling constants of the iodine atom. If we compare the monosubstituted methyl halide systems in Table 2 to the monosubstituted ethyl halides in Table 3, they are in excellent agreement of each other. This is expected, given that the molecular structure is similar. It only deviates by the extra methyl group. Although the approach for these molecules is very different when studying them in rotational spectroscopy. The methyl halides are symmetrical rotors, while the ethyl halides are treated as asymmetrical rotors.

Molecular systems that have two halides or more have posed a challenge on the rotational spectrum due to the two nuclear magnetic moments. This is important because the nuclear magnetic moments from both nuclei will couple to each other causing the rotational transition to be split into dozens of lines. Because the project in this thesis has two halides, I will discuss molecules that have been previously studied by several groups to understand these species more. With the information that was obtained from monosubstituted halides, rotational spectroscopists expanded to dihalide methanes. Myers *et al.* first assigned the complete structure analysis and the diagonalized matrix elements of $CH_2Cl_2$ and its isotopomers [69]. They concluded the H-C-H to be 112°58’ and the Cl-C-Cl to be 111°47’, which is a little off compared to what was observed in the monosubstituted halomethanes, and concluding that the Cl-C-Cl bond is bent [69]. Flygare *et al.* reinvestigated this molecule and determined the off-diagonal terms along with the Cl-C-Cl bond angle not being bent [92]. Chadwick *et al.* obtained the rotational spectrum at high *J* quantum numbers of $CH_2Br_2$ along with is isotopomers [23]. They determined a full structural analysis and the diagonal and off-diagonal terms of the nuclear quadrupole coupling constants of all 4 isotopomers, $CH_2{}^{79}Br_2$, $CH_2{}^{81}Br_2$, $CD_2{}^{79}Br_2$, and $CD_2{}^{81}Br_2$ [23-24]. Because there are two Br atoms with a large nuclear quadrupole moment that couple to the molecule’s rotation, the rotational transitions has a large splitting pattern that ranges up to 350 MHz A similar study was performed on the $CH_2I_2$ molecular system, where Kisiel and coworkers had a bit of trouble assigning its rotational spectrum [103]. Because the nuclear magnetic moments of both iodine atoms are large and interact with each and the molecular rotation, every rotational transition will be split almost 2 GHz wide [103]. Therefore, when they tried assigning the spectrum on one spectrometer, they could not determine a good assignment due to the fact that they were dealing with large $J$ quantum numbers. It was not until they combined the power of room temperature and super-sonic expansion techniques that they were able to determine the structure [103]. Which lead them to conclude the bond length for the $CH_2X_2$ series get longer, as was reported in the past by the monosubstituted methyl halides series. For the initial treatment of the nuclear quadrupole coupling constants, they scaled the diagonalized nuclear quadrupole constants of the $CH_3I$ and the $\chi_{zz}$ [$CH_2Br_2$]/ $\chi_{zz}$ [$CH_3Br$]. They then flipped the constant to be on the same axis as the principal axis and the angle between the $a$-axis of the $CH_2I_2$ and the C-I bond [103]. Which allowed a better treatment of the diagonal terms of the nuclear quadrupole constants. Even then, few uncertainties on the off-diagonal terms which could have helped fit some unassigned splittings [103]. They also made a comparison to the lighter halogen series and their nuclear quadrupole constants to the dihalide methanes and their nuclear quadrupole coupling constants. Which they conclude the increase of the halide size, would prompt a larger ratio of $\chi_{zz}$ and the angle of the <XCX to increase also, which as they reported is larger than that of a tetrahedral 109.5° [103]. Although these methyl halide/dihalide systems gave vital information on the structure and behavior of the nuclear quadrupole coupling constants, they do not quite compare to the system that this project is studying.

A molecule that is closely related to 1,1-diiodoethane and has been studied immensely by various research groups in the microwave spectroscopy community is 1,1-dichloroethane. The first partial structural and quadrupole hyperfine coupling constants assignment of this molecule was made by Flygare [104]. Where the bond angle of <Cl-C-Cl was calculated to be 112°0', which is a bit more than what has been seen in Table 2 and Table 3 [93]. This also means that there is a strain on the $sp^3$ hybridized carbon. Sugie *et al.* was able to get a complete structural determination of 1,1-dichloroethane, 1,2-dichloroethane, and 1,1,1-trichloroethane [53]. Although no 1,1-dibromoethane, 1,2-dibromoethane, and even 1,2-diiodoethane, has been rotationally studied, they are as equally important and would give a lot of information in terms of molecular structure and nuclear quadrupole coupling constants.

The rotational spectrum of any diiodine containing molecule has posed quite a challenge. Only a handful of these molecules have been rotationally tackled. The first one was diiodomethane and its deuterated species [103,104]. Followed by difluorodiiodomethane, which was studied by Grubbs *et al.* and remains unsolved [33]. Another molecular system that bared quite a challenge and was the first halosilane with two halides to be rotationally studied was, diiodosilane [28]. Where the assignment of this molecule gave detailed information on the molecular geometry, nuclear quadrupole coupling constants, and the nature of the Si-I bond [28]. The reason only a handful of diiodine containing species have been studied is because of the nuclear quadrupole coupling of the two iodine are large. One iodine's nuclear quadrupole moment will couple to the other nuclear quadrupole moment and then couple to the molecule's rotation. Causing the rotational transition to be split 500 MHz or more. This spacing makes it difficult to assign any rotational transition with 100 % confidence. Rendering these systems more difficult than the dihalomethanes and dihaloethane systems. Another reason is the nuclear spin-rotation shifting. If these values are larger than they will contribute a large shifting pattern.

## 4.2 *Ab initio* Calculations

A potential energy surface scan (Fig. 15) was implemented along the I-C-C-H dihedral angle at 36 steps every 10 degrees at the MP2/aug-cc-pVTZ-pp levels. Because both carbons are tetrahedral conformations, the PES scan yields a 3-fold minima and maxima as shown in Fig. 15.

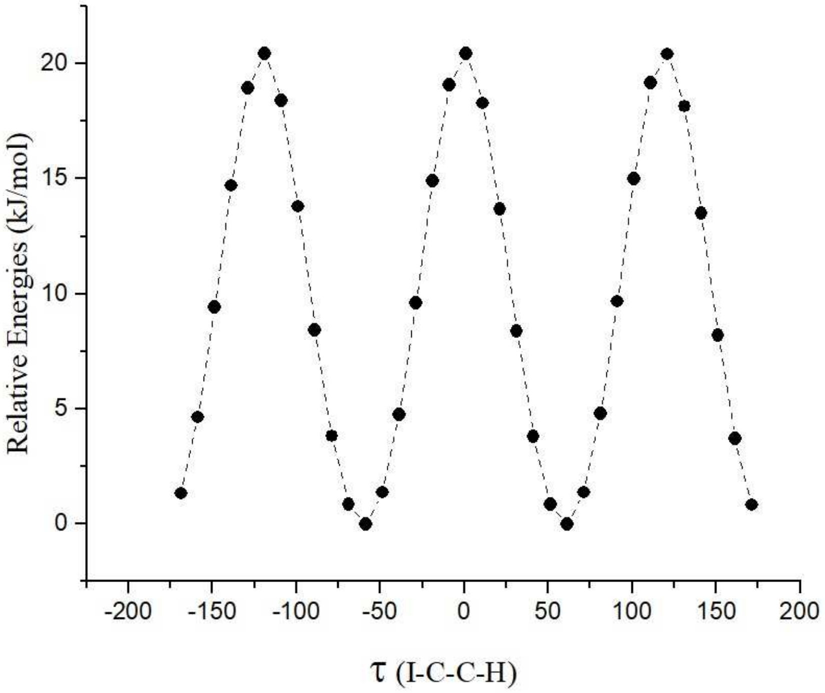

Figure 15. Shows the PES scan at MP2/aug-cc-pVTZ-pp level

The 3-fold minima shows that there is only one conformation for this molecular system. It also shows a potential energy barrier height of 20 kJ/mol. The global minima was then optimized at the CCSD(T) level along with the aug-cc-pVTZ-pp basis set using Molpro [51]. The -pp was taken from the online basis set exchange website, which was used to account for the d- electrons in the iodine atoms. [6]. This produced the equilibrium structure along with its calculated bond angles and bond lengths as shown in Table 4 and Fig. 16 (top). From this calculation we were also able to obtain the inertial axis location as shown in Fig. 16 (bottom). The structure was then re-calculated by single-point calculation at the MP2/ aug-cc-pVTZ-pp basis set using Gaussian 16 (G16) [79].

Because Molpro could not produce the nuclear quadrupole coupling and nuclear spin-rotation constants for the iodine atoms, G16 was utilized to produce them. Table 4 shows the bond angles, bond length, and dihedral angles. Where the R represents the bond length, A represents angle between bonds, and D represents dihedral angle. Comparing the calculated C-I bond to the one found in literature, the calculated C-I bond is much shorter [104]. Another full re-optimization was performed at the MP2/aug-cc-pVTZ-pp level in order to compare structure parameter (showed in Table 4), rotational, dipole moments, nuclear quadrupole coupling, and nuclear spin-rotation constants (shown in Table 5) to the higher-level calculation.

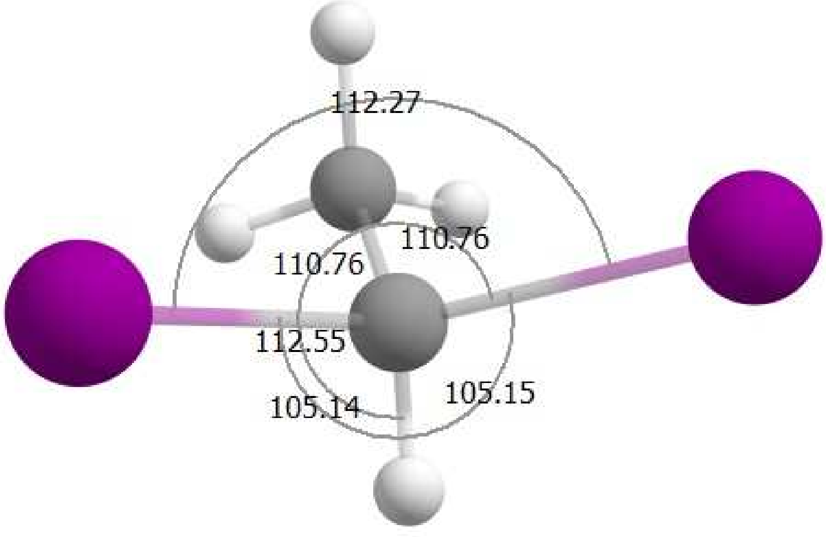

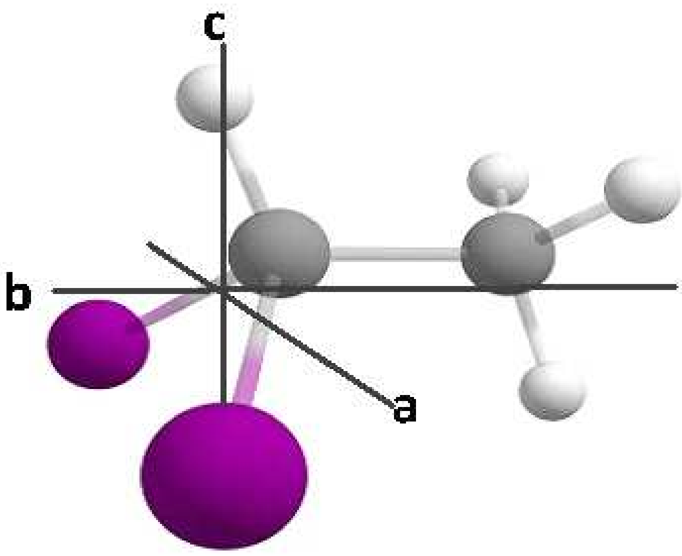

Figure 16. Shows 1,1-diiodoethane's calculated from CCSDT/aug-cc-pvtz-pp bond angles and bond lengths (top) along with its inertial axis(bottom).

| **Parameter** | **Bond length (Å) and bond angles (degree)** | |
|---|---|---|
| | CCSD(T)/aug-cc-pVTZ-pp | MP2/aug-cc-pVTZ-pp |
| **$R_{C\text{-}C}$** | 1.516 Å | 1.510 Å |
| **$R_{C\text{-}H}$** | 1.085 Å | 1.084 Å |
| **$A_{C\text{-}C\text{-}H}$** | 112.4° | 112.5° |
| **$R_{C\text{-}I}$** | 2.145 Å | 2.132 Å |
| **$A_{H\text{-}C\text{-}I}$** | 105.1° | 105.1° |
| **$D_{C\text{-}C\text{-}H\text{-}I}$** | 120.5° | 120.6° |
| **$R_{C\text{-}I}$** | 2.147 Å | 2.133 Å |
| **$A_{H\text{-}C\text{-}I}$** | 105.1° | 105.1° |
| **$D_{C\text{-}C\text{-}H\text{-}I}$** | 120.5° | 120.6° |
| **$R_{C\text{-}H}$** | 1.092 Å | 1.090 Å |
| **$A_{C\text{-}C\text{-}H}$** | 109.7° | 109.6° |

| | | |
|---|---|---|
| **$D_{H-C-C-H}$** | 59.9° | 59.9° |
| **$R_{C-H}$** | 1.092 Å | 1.090 Å |
| **$A_{C-C-H}$** | 109.7° | 109.9° |
| **$D_{H-C-C-H}$** | 59.9° | 59.9° |
| **$R_{C-H}$** | 1.091 Å | 1.088Å |
| **$A_{C-C-H}$** | 110.8° | 110.7° |
| **$D_{H-C-C-H}$** | 179.9° | 179.9° |

Table 4. Shows the calculated structure parameters of 1,1-diiodoethane at the CCSD(T) and MP2 level.

| **Parameters** | **CCSD(T)/aug-cc-pVTZ-pp** | **MP2/aug-cc-pVTZ-pp** |
|---|---|---|
| **$A$ (MHz)** | 4514.700 | 4492.281 |
| **$B$ (MHz)** | 601.277 | 603.198 |
| **$C$ (MHz)** | 538.697 | 540.377 |
| **$\mu_a$ (Debye)** | 0.0 | 0.0 |
| **$\mu_b$ (Debye)** | 1.8 | 1.8 |
| **$\mu_c$ (Debye)** | 0.5 | 0.5 |
| **$\chi_{aa}$ (MHz)** | -1505.176 | -1472.092 |
| **$\chi_{bb}- \chi_{cc}$ (MHz)** | -118.821 | -110.140 |
| **$\chi_{ab}$ (MHz)** | -1063.464 | 1049.430 |
| **$\chi_{ac}$ (MHz)** | 460.757 | 504.698 |
| **$\chi_{bc}$ (MHz)** | 269.887 | -294.384 |
| **$C_{aa}$ (kHz)** | 0.005 | 0.005 |

| | | |
|---|---|---|
| **$C_{bb}$ (kHz)** | 0.002 | 0.002 |
| **$C_{cc}$ (kHz)** | 0.002 | 0.002 |
| **$C_{ab} + C_{ba}$ (kHz)** | -0.003 | 0.003 |
| **$C_{ab} + C_{ba}$ (kHz)** | 0.002 | -0.002 |
| **$C_{ac} + C_{ca}$ (kHz)** | 0.001 | -0.001 |
| **$C_{ac} - C_{ca}$ (kHz)** | -0.001 | 0.001 |
| **$C_{bc}+C_{cb}$ (kHz)** | 0.0002 | 0.0002 |
| **$C_{aa}$ (kHz)** | -0.0006 | -0.0006 |
| **$C_{aa}$(kHz)** | -0.0001 | -0.0001 |
| **$C_{ab} + C_{ba}$ (kHz)** | -0.0001 | -0.0001 |
| **$C_{ab} - C_{ba}$ (kHz)** | 0.0001 | 0.0001 |

Table 5. shows calculated spectroscopic parameters from CCSD(T) and MP2 calculations.

It has been noted in the past that the nuclear quadrupole constants of iodine containing systems are extremely large as evidenced in Table 5. The rotational and nuclear quadrupole coupling constants were utilized to predict the simulated rotational spectrum as seen in Fig. 18.

### 4.3 Internal Rotation

Whenever molecules have a terminal methyl group on them, they may experience free rotation about the C-C bond. Since the hydrogens on the methyl group are so light, it allows this motion to happen depending on the energy relative to the potential energy barrier ($V_3$). Internal rotation results in the splitting of the vibrational states, which split into the A and two degenerate E states as shown in Fig. 17.

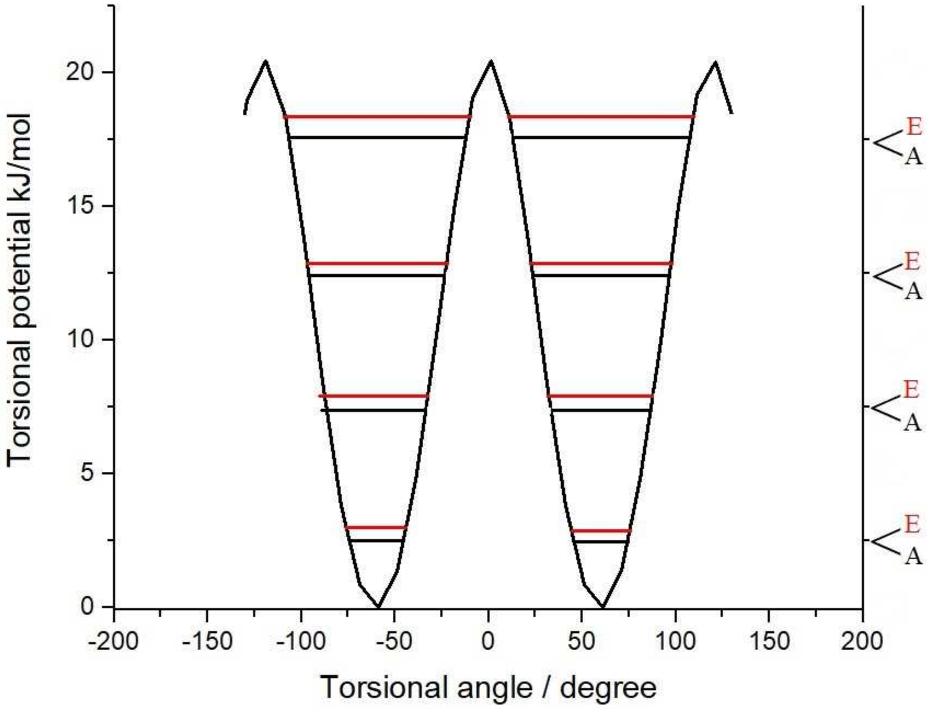

Figure 17. Shows a generic $V_3$ potential energy barrier along with the two vibrational states being split.

Where the A state is less perturbed and treated almost regularly, and the E state is the doubly degenerate state. In order to treat the E state, we must have information on the barrier height potential. I will discuss briefly about the potential barrier height and how it pertains to 1,1-diiodoethane. Several studies have been performed on methyl containing molecules in order to be able to determine the barrier height of the rotation about the C-C bond [79,40,99,30,7]. Table 5 shows the comparison of the calculated barrier height of 1,1-diiodoethane and other experimentally solved molecules. One can see that there would be internal rotation for molecules with a very low barrier like1,1-difluoroethane. This would be extremely difficult because perturbation theory must be utilized in order to treat the E state. For instance, A. de Luis *et al.* observed a small internal rotation splitting in the low-lying vibrationally excited state of 1,1-dichloroethane [3].

| Molecule | $V_3$ (kJ/mol) |
|---|---|
| **1,1-difluoroethane** | 13.94 |
| **Ethyl Fluoride** | 14.07 |
| **Ethyl Chloride** | 15.13 |
| **Ethyl Iodide** | 15.20 |
| **Ethyl Bromide($^{79}$Br)** | 15.32 |
| **Ethyl Bromide($^{81}$Br)** | 15.41 |
| **1,2-dichloroethane** | 17.89 |
| **1,1-dichloroethane** | 17.90 |
| **1-chloro-1,1-difluoroethane** | 18.48 |
| **1,1-diiodoethane** | ~20.00 |

Table 6. Shows the different $V_3$ measured through rotational spectroscopy.

This molecules structure resembles 1,1-diiodoethane, but instead of having two iodine atoms, it contains two chlorine atoms. Because the possible interactions of the two iodine atoms with the three hydrogen atoms on the methyl group, there could be a possibility that there is or is not internal rotation in 1,1-diiodoethane. The experimental $V_3$ potential barriers reported in Table 6 show that systems related to 1,1-diiodoethane have barrier heights close to the calculated value of 20 kJ/mol. Therefore, internal rotation may be seen experimentally.

### 4.4 Analysis

When two iodine atoms are added onto an ethane molecule, the rotational spectrum becomes even more complicated to fit. As seen in Table 4, the nuclear quadrupole coupling constants from CCSD(T) calculation are a lot larger than that of the rotational constants. Thus, the simulated rotational spectrum shown in Fig. 18 denotes the complexity. Fig. 16 and Table 5 also shows that there is no dipole moment on the a- axis. Therefore, no a- type rotational transitions will be observed, only the strong b- type and weak c- type transitions. When the rotational spectrum was experimentally recorded for the most part of the 11-18 GHz range (shown in Fig. 18, we did not scan from 12.5-13.5 GHz region.), it seemed to line up with the fact that the nuclear quadrupole coupling constants are larger than that of the $B$ and $C$ rotational constants. Meaning that the rotational spectrum is more dependent on the splittings due to the nuclear quadrupole coupling of the two iodine atoms than that of the rotational transitions.

In order to fit the rotational spectrum, we utilized Pickett's program for fitting and simulating the rotational spectrum [35]. The Hamiltonian operator applied to 1,1-diiodoethane is:

$$\widehat{H} = \widehat{H}_R + \widehat{H}_{CD} + \widehat{H}_{NQC} + \widehat{H}_{NSR} \tag{78}$$

where the Hamiltonians operator that was discussed in chapter 1, is not being utilized since the molecule has all these features. Recall that the $\widehat{H}_R$ pertains to the rotational Hamiltonian of rigid rotor; the $\widehat{H}_{CD}$ is for the centrifugal distortion; the $\widehat{H}_{NQC}$ pertains to the nuclear quadrupole coupling; the $\widehat{H}_{NSR}$ represents the nuclear spin-rotation coupling. These features will be discussed in the later section but are important because of the magnitude that they pose in the rotational spectrum. Two types of coupling schemes were considered for fitting the spectrum, consequential and sequential. In both occasions the quantum label produced is $J''k_a''k_c''F_1''F'' \rightarrow J'k_a'k_c'F_1'F'$. Both coupling schemes will give identical final positions of the rotational transitions.

Since both iodine atoms bisect the b-axis in Fig. 16 (bottom), the nuclear quadrupole and nuclear spin-rotation constants can be treated symmetrically. Meaning only one set of hyperfine constants would be taken into consideration in the fit. This symmetry significantly reduces the complexity of the spectrum analysis. This is how other previously studied dihalogen methanes/ethanes were confronted and solved. If both iodine atoms were not symmetrical it would make the hyperfine constants extremely hard and the rotational spectrum nearly impossible to solve.

### 4.4.1 Sequential coupling Scheme

We utilized the sequential coupling scheme for the beginning of this experiment. This scheme is shown in equation(s) 79 & 80.

$$F_1 = I_1 + J \tag{79}$$

$$F = I_2 + F_1 \tag{80}$$

where $I_1$ and $I_2$ are both $\frac{5}{2}$ . When we couple the nuclear magnetic moment to $J$ which represents the rotational angular momentum quantum number, we obtain the total angular momentum ($F_1$). We then couple $F_1$ to the second nuclear magnetic moment of the second iodine and obtain $F$. By using this coupling scheme, we were able to obtain a root-mean-square error (RMS) of approximately 0.7 MHz. Resulting in a simulating spectrum that lines up very nicely with the experimental one and is shown in Fig. 18. This is initially a good indication that the fit is in the right direction. However, the satisfactory fitting error should match the experimental error of about 2-5 kHz, indicating that there is still major progress needed.

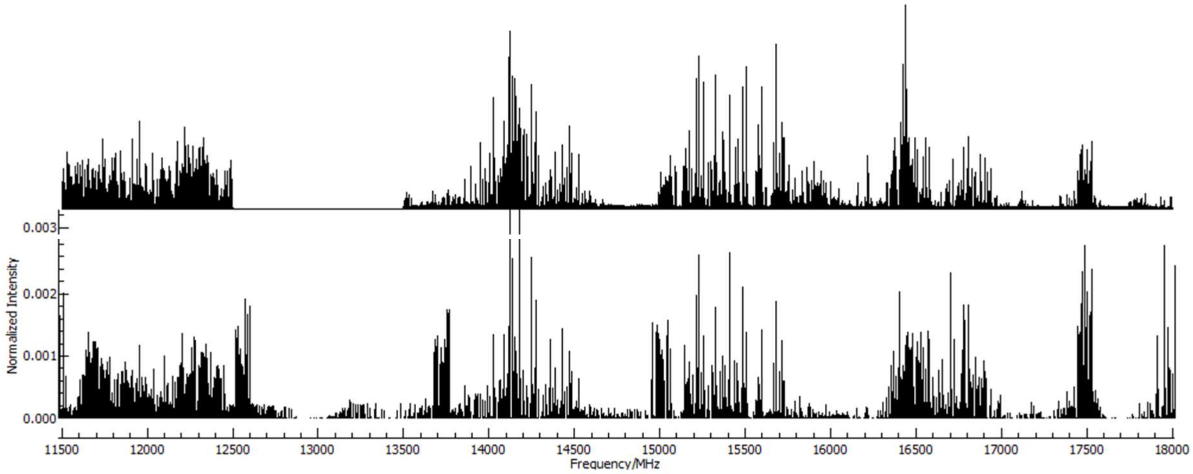

Figure 18. Shows the experimental (top) and predicted (bottom) rotational spectrum of 1,1-diiodoethane with a fitting of 0.7 MHz

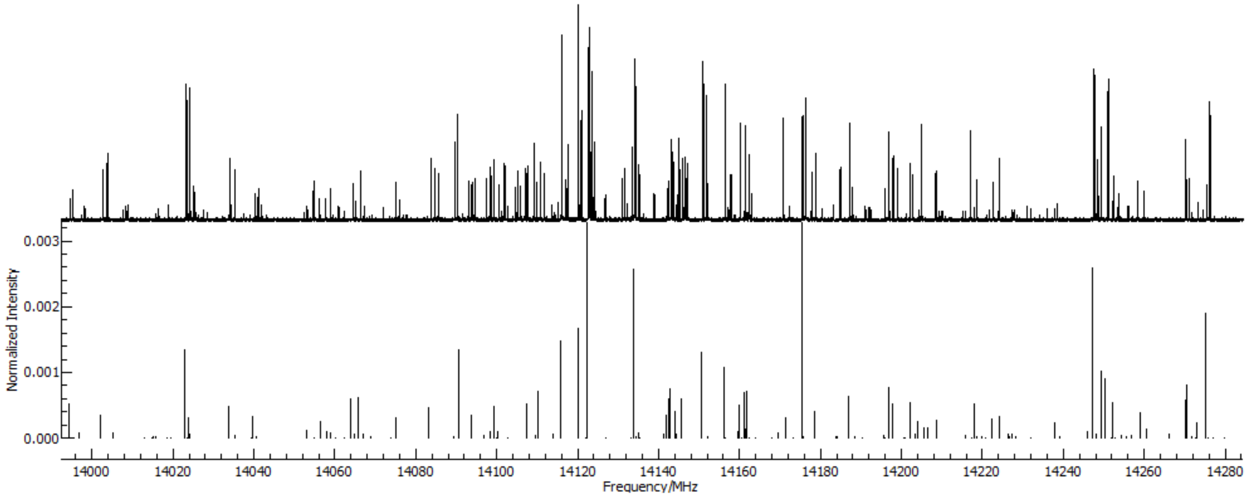

Figure 19. Shows a zoomed in spectrum of 1,1-diiodoethane.

Although once we zoom into the spectrum (Fig. 19) as seen in Fig. 18, we notice some discrepancies. In addition, there are more experimental lines than the ones seen in the prediction. This is a strong indication that there is internal rotation. Although with our preliminary fit, we cannot determine for certain. Further improvement of the RMS error would help provide such information.

| **Parameter** | **Experimental Constants** | **CCSD(T)/aug-cc-pVTZ-pp** |
|---|---|---|
| ***A* (MHz)** | 4476.(30) | 4514.700 |
| ***B* (MHz)** | 607.(6) | 601.277 |
| ***C* (MHz)** | 569.(2) | 538.697 |
| **$\Delta_J$(kHz)** | -0.231 | - |
| **$\Delta_{JK}$ (kHz)** | 1.34 | - |
| **$\Delta_K$ (kHz)** | 13.12 | - |

| | | |
|---|---|---|
| **$d_j$ (kHz)** | -0.180 | - |
| **$d_k$ (kHz)** | 7.418 | - |
| **$\chi_{aa}$ (MHz)** | -1636.(2) | -1505.176 |
| **$\chi_{bb}$- $\chi_{cc}$ (MHz)** | -136.7(6) | -118.821 |
| **$\chi_{ab}$ (MHz)** | -1196.(5) | -1063.464 |
| **$\chi_{ac}$ (MHz)** | 544.(7) | 460.757 |
| **$\chi_{bc}$ (MHz)** | 340.(2) | 269.887 |
| ***N*** | 78 | - |
| **σ (kHz)** | 0.7 | - |

*N*[*] is number of fitted lines

Table 7. shows the experimental spectroscopic parameters after the sequential fitting.

The fitted spectroscopic constants from that fit are shown in Table 7. Table 8 shows all of the assigned hyperfine components along rotational transitions.

| J' | Ka' | Kc' | $F_1$' | $F_2$' | J" | Ka" | Kc" | $F_1$" | $F_2$" | $\nu_{EXP}$ / MHz | $\Delta\nu^a$ / MHz |
|---|---|---|---|---|---|---|---|---|---|---|---|
| 2 | 2 | 1 | 9/2 | 7 | 1 | 1 | 0 | 9/2 | 6 | 14120.230 | -2.097 |
| 2 | 2 | 1 | 7/2 | 6 | 1 | 1 | 0 | 7/2 | 6 | 14134.273 | 0.434 |
| 2 | 2 | 1 | 7/2 | 5 | 1 | 1 | 0 | 7/2 | 4 | 14151.016 | 0.296 |
| 2 | 2 | 1 | 9/2 | 5 | 1 | 1 | 0 | 9/2 | 5 | 14156.436 | 0.392 |
| 2 | 2 | 0 | 9/2 | 5 | 1 | 1 | 0 | 9/2 | 5 | 14157.856 | -1.634 |
| 2 | 2 | 1 | 1/2 | 3 | 1 | 1 | 0 | 5/2 | 2 | 14160.248 | -0.780 |
| 2 | 2 | 0 | 3/2 | 3 | 1 | 1 | 1 | 3/2 | 2 | 14161.347 | -0.200 |
| 2 | 2 | 0 | 7/2 | 6 | 1 | 1 | 1 | 7/2 | 5 | 14247.629 | 0.625 |
| 2 | 2 | 0 | 3/2 | 4 | 1 | 1 | 1 | 3/2 | 3 | 14251.105 | 1.613 |
| 2 | 2 | 1 | 7/2 | 5 | 1 | 1 | 0 | 7/2 | 5 | 14270.207 | -0.264 |
| 2 | 2 | 0 | 5/2 | 5 | 1 | 1 | 1 | 5/2 | 4 | 14276.216 | 1.367 |
| 2 | 2 | 1 | 9/2 | 5 | 1 | 1 | 0 | 5/2 | 4 | 14351.745 | -0.007 |
| 2 | 2 | 0 | 9/2 | 4 | 1 | 1 | 1 | 5/2 | 4 | 14352.715 | -0.413 |
| 2 | 2 | 0 | 7/2 | 3 | 1 | 1 | 1 | 7/2 | 3 | 14353.223 | -0.664 |
| 2 | 2 | 0 | 7/2 | 5 | 1 | 1 | 1 | 7/2 | 4 | 14359.468 | 0.421 |
| 2 | 2 | 0 | 9/2 | 4 | 1 | 1 | 1 | 5/2 | 3 | 14362.998 | 0.309 |
| 2 | 2 | 0 | 7/2 | 5 | 1 | 1 | 1 | 7/2 | 5 | 14385.152 | 0.952 |
| 2 | 2 | 1 | 1/2 | 3 | 1 | 1 | 0 | 5/2 | 3 | 14400.699 | 0.163 |
| 2 | 2 | 0 | ½ | 3 | 1 | 1 | 1 | 5/2 | 2 | 14458.590 | 0.159 |
| 2 | 2 | 1 | 9/2 | 6 | 1 | 1 | 0 | 9/2 | 6 | 14471.324 | 0.289 |

| | | | | | | | | | | | |
|---|---|---|---|---|---|---|---|---|---|---|---|
| 2 | 2 | 0 | 9/2 | 5 | 1 | 1 | 1 | 9/2 | 5 | 14471.758 | -0.007 |
| 2 | 2 | 0 | 7/2 | 4 | 1 | 1 | 1 | 7/2 | 4 | 14479.211 | 0.156 |
| 2 | 2 | 0 | 7/2 | 4 | 1 | 1 | 1 | 7/2 | 3 | 14481.977 | -0.489 |
| 2 | 2 | 0 | 9/2 | 6 | 1 | 1 | 1 | 9/2 | 6 | 14525.572 | 0.109 |
| 2 | 2 | 1 | 9/2 | 5 | 1 | 1 | 1 | 9/2 | 4 | 14589.004 | -0.668 |
| 3 | 2 | 2 | 5/2 | 6 | 2 | 1 | 1 | 5/2 | 5 | 15169.782 | -0.768 |
| 3 | 2 | 2 | 7/2 | 7 | 2 | 1 | 1 | 7/2 | 6 | 15212.157 | 0.900 |
| 3 | 2 | 2 | 9/2 | 8 | 2 | 1 | 1 | 9/2 | 7 | 15229.943 | 0.565 |
| 3 | 2 | 2 | 7/2 | 5 | 2 | 1 | 1 | 7/2 | 5 | 15255.323 | -0.644 |
| 3 | 2 | 2 | 9/2 | 7 | 2 | 1 | 1 | 9/2 | 6 | 15324.092 | 0.631 |
| 3 | 2 | 2 | 3/2 | 3 | 2 | 1 | 1 | 0 | 2 | 15326.229 | 0.040 |
| 3 | 2 | 1 | 9/2 | 2 | 2 | 1 | 2 | 9/2 | 3 | 15331.999 | -0.133 |
| 3 | 2 | 1 | 9/2 | 8 | 2 | 1 | 2 | 9/2 | 7 | 15407.764 | -0.510 |
| 3 | 2 | 1 | 9/2 | 5 | 2 | 1 | 2 | 9/2 | 4 | 15440.932 | 0.734 |
| 3 | 2 | 2 | 7/2 | 5 | 2 | 1 | 2 | 3/2 | 4 | 15454.743 | -0.066 |
| 3 | 2 | 1 | 7/2 | 4 | 2 | 1 | 2 | 3/2 | 4 | 15464.199 | -0.223 |
| 3 | 2 | 1 | 7/2 | 7 | 2 | 1 | 2 | 7/2 | 6 | 15486.753 | -0.620 |
| 3 | 2 | 1 | 5/2 | 6 | 2 | 1 | 2 | 5/2 | 5 | 15504.003 | -0.777 |
| 3 | 2 | 1 | 5/2 | 5 | 2 | 1 | 2 | 5/2 | 4 | 15579.200 | 0.914 |
| 3 | 2 | 1 | 7/2 | 6 | 2 | 1 | 2 | 7/2 | 5 | 15596.401 | -1.466 |
| 3 | 2 | 1 | 9/2 | 6 | 2 | 1 | 2 | 9/2 | 6 | 15665.564 | 1.3816 |
| 3 | 2 | 1 | 9/2 | 7 | 2 | 1 | 2 | 9/2 | 6 | 15679.752 | -0.895 |
| 3 | 2 | 1 | 3/2 | 3 | 2 | 1 | 2 | 0 | 2 | 15703.391 | 0.561 |
| 3 | 2 | 1 | 5/2 | 4 | 2 | 1 | 2 | 5/2 | 3 | 15715.407 | 0.704 |
| 3 | 2 | 1 | 7/2 | 5 | 2 | 1 | 2 | 7/2 | 4 | 15716.453 | -0.363 |
| 3 | 2 | 1 | 9/2 | 6 | 2 | 1 | 2 | 9/2 | 5 | 15721.157 | 0.936 |
| 3 | 2 | 1 | 5/2 | 6 | 2 | 1 | 2 | 9/2 | 5 | 15729.232 | -1.010 |
| 5 | 2 | 4 | 9/2 | 8 | 4 | 1 | 3 | 9/2 | 8 | 17385.525 | 0.036 |
| 5 | 2 | 4 | 9/2 | 3 | 4 | 1 | 3 | 9/2 | 2 | 17396.240 | -0.361 |
| 5 | 2 | 4 | 7/2 | 7 | 4 | 1 | 3 | 7/2 | 7 | 17410.373 | 0.722 |
| 5 | 2 | 4 | 9/2 | 4 | 4 | 1 | 3 | 9/2 | 3 | 17423.135 | -1.747 |
| 5 | 2 | 4 | ½ | 6 | 4 | 1 | 3 | ½ | 5 | 17445.362 | 1.232 |
| 5 | 2 | 4 | 9/2 | 7 | 4 | 1 | 3 | 9/2 | 7 | 17451.432 | 0.887 |
| 5 | 2 | 4 | ½ | 6 | 4 | 1 | 3 | 9/2 | 6 | 17451.946 | 1.114 |
| 5 | 2 | 4 | ½ | 5 | 4 | 1 | 3 | ½ | 4 | 17455.539 | 0.502 |
| 5 | 2 | 4 | 3/2 | 5 | 4 | 1 | 3 | 3/2 | 4 | 17455.871 | 0.505 |
| 5 | 2 | 4 | 9/2 | 7 | 4 | 1 | 3 | 9/2 | 6 | 17458.260 | 0.781 |
| 5 | 2 | 4 | 0 | 5 | 4 | 1 | 3 | 0 | 4 | 17458.328 | 0.391 |
| 5 | 2 | 4 | 5/2 | 5 | 4 | 1 | 3 | 5/2 | 4 | 17458.693 | 0.105 |
| 5 | 2 | 4 | 9/2 | 8 | 4 | 1 | 3 | 9/2 | 7 | 17465.297 | -0.279 |
| 5 | 2 | 4 | 7/2 | 7 | 4 | 1 | 3 | 7/2 | 6 | 17466.209 | -0.336 |
| 5 | 2 | 4 | 9/2 | 6 | 4 | 1 | 3 | 9/2 | 5 | 17468.010 | 1.049 |
| 5 | 2 | 4 | 7/2 | 5 | 4 | 1 | 3 | 7/2 | 4 | 17471.377 | -1.129 |
| 5 | 2 | 4 | 9/2 | 9 | 4 | 1 | 3 | 9/2 | 8 | 17472.168 | -1.197 |
| 5 | 2 | 4 | 3/2 | 4 | 4 | 1 | 3 | 3/2 | 3 | 17480.074 | -0.933 |
| 5 | 2 | 4 | ½ | 4 | 4 | 1 | 3 | ½ | 3 | 17485.065 | -0.836 |

| | | | | | | | | | | | |
|---|---|---|---|---|---|---|---|---|---|---|---|
| 5 | 2 | 4 | 9/2 | 10 | 4 | 1 | 3 | 9/2 | 9 | 17489.468 | 0.949 |
| 5 | 2 | 4 | 3/2 | 6 | 4 | 1 | 3 | 3/2 | 5 | 17498.815 | 0.166 |
| 5 | 2 | 4 | 5/2 | 6 | 4 | 1 | 3 | 5/2 | 5 | 17500.166 | 0.119 |
| 5 | 2 | 4 | 7/2 | 8 | 4 | 1 | 3 | 7/2 | 7 | 17501.338 | -0.000 |
| 5 | 2 | 4 | 5/2 | 5 | 4 | 1 | 3 | ½ | 5 | 17504.032 | 0.209 |
| 5 | 2 | 4 | 7/2 | 2 | 4 | 1 | 3 | 7/2 | 1 | 17505.980 | 0.164 |
| 5 | 2 | 4 | 5/2 | 3 | 4 | 1 | 3 | 5/2 | 2 | 17508.891 | -1.548 |
| 5 | 2 | 4 | 5/2 | 3 | 4 | 1 | 3 | 5/2 | 2 | 17511.035 | 0.596 |
| 5 | 2 | 4 | 5/2 | 7 | 4 | 1 | 3 | 5/2 | 6 | 17513.568 | -0.395 |
| 5 | 2 | 4 | 3/2 | 7 | 4 | 1 | 3 | 3/2 | 6 | 17520.821 | -0.718 |
| 5 | 2 | 4 | 7/2 | 9 | 4 | 1 | 3 | 7/2 | 8 | 17527.473 | 0.556 |
| 5 | 2 | 4 | 5/2 | 8 | 4 | 1 | 3 | 5/2 | 7 | 17529.072 | -0.681 |
| 3 | 2 | 2 | 9/2 | 8 | 3 | 1 | 3 | 9/2 | 8 | 11952.104 | -0.158 |
| 9 | 2 | 7 | 5/2 | 12 | 9 | 1 | 8 | 5/2 | 12 | 11910.865 | -0.046 |
| 9 | 2 | 8 | 5/2 | 12 | 9 | 1 | 9 | 5/2 | 12 | 11941.037 | 0.0240 |
| 5 | 2 | 3 | 9/2 | 10 | 5 | 1 | 4 | 9/2 | 10 | 11652.892 | -0.143 |
| 6 | 2 | 4 | 9/2 | 11 | 6 | 1 | 5 | 9/2 | 11 | 11655.993 | 0.276 |
| 5 | 2 | 4 | 3/2 | 7 | 5 | 1 | 5 | 3/2 | 7 | 12298.302 | -0.113 |
| 7 | 2 | 6 | 5/2 | 8 | 7 | 1 | 7 | 5/2 | 8 | 12297.426 | -0.017 |
| 7 | 2 | 6 | 3/2 | 8 | 7 | 1 | 7 | 3/2 | 8 | 12297.049 | -0.004 |
| 4 | 2 | 3 | 9/2 | 8 | 3 | 1 | 2 | 9/2 | 7 | 16437.096 | -0.632 |

[a] $\Delta\nu = \nu_{EXP} - \nu_{CAL}$.

Table 8. Observed rotational transition frequencies of the 1,1-diiodoethane.

### 4.4.2 Consequential Coupling Scheme

In the consequential coupling scheme, shown in equation(s) 81 & 82

$$I_{tot} = I_1 + I_2 \tag{81}$$

$$F = I_{tot} + J \tag{82}$$

The use of eq. 81 couples the two nuclear spins together first to obtain a total nuclear spin quantum number. Eq. 82 couples the total nuclear spin to the rotational angular momentum quantum number to produce a total angular momentum quantum number (*F*). The advantage of this coupling scheme is that the coupling of the two iodine nuclear spins may produce a scheme with $I_{tot}$ being zero. When the $I_{tot}$ is zero, *F* is equal to *J*, and the rotational transition can be treated like systems that do not have nuclear spin(s). Thus, producing a quantum label like eq. 22. The benefit to using this scheme is that it would allow us to obtain a fit of 5 kHz and better rotational and centrifugal distortion constants than that of the current sequential coupling scheme. We would then take the fitted rotational and centrifugal distortion constants and plug them into the sequential coupling scheme. We would fix them and only focus on fitting the nuclear quadrupole coupling and nuclear spin-rotation constants.

## 4.5 Conclusion

Alkyl halides are anthropogenic molecules that have been detected all over the world. They pose a threat to the ozone layer, harvest, and all life on earth. Several important alkyl halides have been studied by rotational spectroscopists. The purpose was to obtain a better understanding of the structure of these molecular systems along with their hyperfine components. Since the structure is related to energy, one can understand how energetic they are in the environment, ground water, and atmosphere and come up with a mechanism to get them out of that medium. The rotational spectrum and nuclear hyperfine coupling constants of 1,1-diiodoethane were investigated for the first time by jet pulsed cavity-based FTMW spectrometer. High level *ab initio* calculations provided a better understanding of the structure of 1,1-diiodoethane and its nuclear hyperfine structure, which aided in the experimental search. The use of sequential coupling scheme allowed us to obtain a RMS error of 0.7 MHz. This means that our initial fit is contaminated by the hyperfine splittings. The plan is to use the consequential coupling scheme and obtain a fit of 2-5 kHz From that fit, we would take the fitted rotational and centrifugal distortion constants and plug them into the sequential coupling scheme. Allowing the rotational and centrifugal distortion constants to be fixed and only focusing on the hyperfine components. At this time internal rotation cannot be ruled out as a possibility, it is highly suspected, given the $V_3$ barrier heights being close to the calculated one.

# REFERENCES

[1] A. Alabdulhadi, A. Ramadan, P. Devey, M. Boggess, M. Guest, J. Air Waste Mang. Assoc. 10, 69, 2019.

[2] A. Dubrulle, D. Boucher, J. Burie, J. Demasion, Chem. Phys. Lett. 45, 559, 1977.

[3] Ana de. Luis, J. C. López, J. L. Alonso, Chem. Phys. 248, 247, 1999.

[4] A. Innes, J. Innes, “Flame Retardants”, Applied plastic in Engineering Handbook, 2011.

[5] A. Serrato III, Experimental and Computational Studies in and Proton Tunneling in Organic Molecules and Dimers, Thesis, University of Texas Rio Grande Valley,2018.

[6] “Basis set Exchange”, https://www.basissetexchange.org/, Accessed August 25, 2020.

[7] B. Boucher, A. Dubrulle, J. Demaison, Z. Natur. 35a, 442, 1980.

[8] B. C. Dian, G. G. Brown, K. O. Douglass, B. H. Pate, Science 320, 924, 2008.

[9] B. Gal, C. Bucher, N. Z. Burns, Mar. Drugs, 14, 206, 2016.

[10] “Cameo Chemicals”, NOAA, https://cameochemicals.noaa.gov/chemical/3864, Accessed April 6,2020.

[11] C. Brand, Shaping and Modeling Electronically Excited States of Indoles, Heinrich-Heine-Universitat Dusseldorf, Thesis, 2013.

[12] C. Cabezas, Y. Endo, PCCP. 33, 18029-18408, 2019.

[13] C. Cabezas, Y. Endo, Spcetroscopic Characterization of the Reaction Products between HCl and the Simplest Criegee Intermediate $CH_2OO$, International Symposium on Molecular Spectroscopy,. http://hdl.handle.net/2142/97138, 2017.

[14] C. D. Sherrill, An introduction to Hartree-Fock Molecular Orbital Theory, June, 2000.

[15] C. E. Cleeton and N. B. Williams, Phys. Rev. 45, 234, 1934.

[16] C. E. Hobbs, Polymers, 224, 11, 2019.

[17] C. Flanagan, L. Pierce, J. Chem. Phys. 38, 2963, 1963.

[18] C. H. Townes, A. L. Schawlow, Microwave Spectroscopy Dover Publication, Inc. 2012.

[19] C. J. Cramer, Essentials of Computational Chemistry: Theories and Models. 2nd Ed. Wiley & Sons, 2004.

[20] C. Møller, M. S. Plesset, Phys. Rev. 46, 0618, 1934.

[21] D. A. McQuarrie, Quantum Chemistry, University Science Books, 2007.

[22] D. Boucher, J. Burie, D. Dangoisse, J. Demaison, A. Dubrulle, Chem. Phys. 29, 322, 1978.

[23] D. Chadwick and D. J. Millen, Chem. Phys. Lett. 5, 7, 1970.

[24] D. Chadwick and D. J. Millen, Trans. Faraday. Soc. 67, 1539, 1971.

[25] D. R. Hartree, Math. Proc. Camb. Phil. Soc. 24, 89, 1928.

[26] D. Qin, Atm. Env. 41, 8424, 2007.

[27] D. Yuan, Z. He, G-P. Yang, Mar. Pollu. Bull. 140, 227, 2019.

[28] E. A. Arsenault, D. A. Obenchain, W. Orellana, S. E. Novick, J. Mol. Spec. 338, 72-76, 2017.

[29] F. J. Lovas, P. H. Krupenie, Microwave spectra of molecules of astrophysical interest VII. carbon monoxide, carbon monosulfide, and silicon monoxide. J. of Phys. And Chem. Ref. Data 3, 245, 1974.

[30] G. Allen, P. N. Brier, G. Lane, Trans. Fara. Soc. 63, 1967.

[31] Gaussian 16, Revision C.01, M. J. Frisch, G. W. Trucks, H. B. Schlegel, G. E. Scuseria, M. A. Robb, J. R. Cheeseman, G. Scalmani, V. Barone, G. A. Petersson, H. Nakatsuji, X. Li, M. Caricato, A. V. Marenich, J. Bloino, B. G. Janesko, R. Gomperts, B. Mennucci, H. P. Hratchian, J. V. Ortiz, A. F. Izmaylov, J. L. Sonnenberg, D. Williams-Young, F. Ding, F. Lipparini, F. Egidi, J. Goings, B. Peng, A. Petrone, T. Henderson, D. Ranasinghe, V. G. Zakrzewski, J. Gao, N. Rega, G. Zheng, W. Liang, M. Hada, M. Ehara, K. Toyota, R. Fukuda, J. Hasegawa, M. Ishida, T. Nakajima, Y. Honda, O. Kitao, H. Nakai, T. Vreven, K. Throssell, J. A. Montgomery, Jr., J. E. Peralta, F. Ogliaro, M. J. Bearpark, J. J. Heyd, E. N. Brothers, K. N. Kudin, V. N. Staroverov, T. A. Keith, R. Kobayashi, J. Normand, K. Raghavachari, A. P. Rendell, J. C. Burant, S. S. Iyengar, J. Tomasi, M. Cossi, J. M. Millam, M. Klene, C. Adamo, R. Cammi, J. W. Ochterski, R. L. Martin, K. Morokuma, O. Farkas, J. B. Foresman, and D. J. Fox, Gaussian, Inc., Wallingford CT, 2016.

[32] G. G. Brown, B. C. Dian, K. O. Douglass, S. M. Geyer, S. T. Shipman, B. H. Pate, Rev. Sci. Instru. 79, 053103, 2008.

[33] G. S. Grubbs, S. A. Cooke, Manuscript in prep 2017.

[34] H.-J. Li, Y. Yokouchi, H. Akimoto, Y. Narita, Geochem. J. 35, 137, 2001.

[35] H. M. Pickett, J. Mol. Spec. 148, 371, 1991.

[36] H. W. Kroto, Molecular Rotation Spectra Dover, 1992.

[37] "Hydrofluorocarbons", Climate & Clean Air Coalition, https://www.ccacoalition.org/fr/slcps/hydrofluorocarbons-hfc, January 1,1970. Accessed March 28, 2020.

[38] J. Demaison, A. Dubrulle, D. Boucher, J. Burie, J. Chem. Phys. 67, 254, 1977.

[39] J. Gripp, H. Dreizler, Zeit. Natur. 43a, 971, 1988.

[40] J. Gripp, H. Dreizler, R. Schwarz, Z. Natur. 40a, 575, 1985.

[41] J. K. J. Watson, Chem. Phys. 48, 4517, 1968,

[42] J. Kraitchman, Am. J. Phys. 21, 17, 1953.

[43] J. Stoll, J. Vrabec, H. Hasse, J. Chem. Phys. 21, 119, 2003.

[44] J. W. Simmons, J. Chem. Phys. 20, 1, 1952.

[45] L. Xue, T. Wang, I. J. Simpson, A. Ding, J. Gao, D. R. Blake, X. Wang, W. Wang, H. Lei, D. Jin, Atm. Env. 45, 6501, 2011.

[46] M. Born, R. Oppenheimer, Ann. Physik, 84,457, 1927.

[47] M. B. McElroy, S. C. Wofsy, J. E. Penner, J. C. McConnel, J. Atmos. Sci. 31, 287, 1974.

[48] M. Deinzer, F. Schaumburg, E. Klein, Environ. Health Perspet., 209, 239, 1978.

[49] M. J. Molina, F.S. Rowland, Nat. 249, 811, 1974.

[50] "Microwave Rotational Spectroscopy", Chemistry LibreTexts, https://chem.libretexts.org/Bookshelves/Physical_and_Theoretical_Chemistry_Textbook_Maps/Supplemental_Modules_(Physical_and_Theoretical_Chemistry)/Spectroscopy/Rotational_Spectroscopy/Microwave_Rotational_Spectroscopy, May 19, 2020, ( Accesed August 30, 2019).

[51] MOLPRO is a package of *ab initio* programs written by H.-J. Werner, P. J. Knowles, G. Knizia, F. R. Manby, M. Schütz, P. Celani, W. Györffy, D. Kats, T. Korona, R. Lindh, A. Mitrushenkov, G. Rauhut, K. R. Shamasundar, T. B. Adler, R. D. Amos, S. J. Bennie, A. Bernhardsson, A. Berning, D. L. Cooper, M. J. O. Deegan, A. J. Dobbyn, F. Eckert, E. Goll, C. Hampel, A. Hesselmann, G. Hetzer, T. Hrenar, G. Jansen, C. Köppl, S. J. R. Lee, Y. Liu, A. W. Lloyd, Q. Ma, R. A. Mata, A. J. May, S. J. McNicholas, W. Meyer, T. F. Miller III, M. E. Mura, A. Nickla, D. P. O'Neill, P. Palmieri, D. Peng, K. Pflüger, R. Pitzer, M. Reiher, T. Shiozaki, H. Stoll, A. J. Stone, R. Tarroni, T. Thorsteinsson, M. Wang, M. Welborn .

[52] M. O. Andreae, Atmos. Chem. Phys. 19, 8523, 2019.

[53] M. Sugie, M. Kato, C. Matsumura, H. Takeo, J. of Mol. Struc. 413, 487, 1997.

[54] NASA, "Chlorofluoromethanes and the Stratosphere", 1, 1977.

[55] NASA, JPL pub. JP, 1, 1977.

[56] N. Garcia-Vaquero, E. Lee, R. J. Castaneda, J. Cho, J. A. Lopez-Ramirez, Desalin. 347, 94, 2014.

[57] "Ozone Hydrocarbons", Iowa State University, http://agron-www.agron.iastate.edu/courses/Agron541/classes/541/lesson14b/14b.3.html, Accessed June 3,2020.

[58] "Ozone-Protection Treaty Had Climate Benefits, Too, Study Says", Earth Institute, https://www.earth.columbia.edu/articles/view/3113, August 5, 2013.

[59] P. Atkins, J. de Paula, Physical Chemistry Thermodynamics, Structure, and Change, W. H Freeman and Company, 2014.

[60] P. F. Bernath, Spectra of atoms and molecules oxford,2005.

[61] P. H. Taylor, B. Dellinger, Environ. Sci. Tech, 22, 438, 1988.

[62] P. J. Crutzen, I. S. A. Isaksen, J. R. McAfee, J. Geophys. Resear., 83,68, 1978.

[63] P. J. Crutzen, I. S. Isaken, J. R. McAfee, J. Geophys. Resear. 83, 71, 1978.

[64] R. Atkinson, Chem. Rev. 85, 69, 1985.

[65] R. D. Flotard, "Sampling and Analysis of Trace-organic Constituents in Ambient and Workplace Air at Coal Conversion Facilities", U. S. Department of Energy.

[66] R. H. Schwendemann, G. D. Jacobs, J. Chem. Phys., 5, 36, 1962.

[67] R. J. Bartlett, G. D. Purvis III, Int. J. Quantum Chem. 14, 561, 1978.

[68] R. J. Cicerone, R. S. Stolarski, S. Williams, Science. 185, 1165, 1974.

[69] R. J. Myers, W. D. Gwinn, J. Chem. Phys. 9, 20, 1952.

[70] R. Nave, "Eigenvalues and Eigenfunctions, Hyperphysics, http://hyperphysics.phy-astr.gsu.edu/hbase/quantum/eigen.html, (Accessed March 15, 2020).

[71] R. S. Wagner, B. P Dailey, J. Chem. Phys. 26, 1588, 1957.

[72] R. S. Wagner, B. P Dailey, N. Solimene, J. Chem. Phys., 6, 26, 1957.

[73] S. C. Wofsy, Mi. B. McElroy, N. D. Sze, Sci. 187, 535, 1975.

[74] S. G. Kukolich, A. C. Nelson, J. Am. Chem. Soc. 95, 3, 1973.

[75] S. H. Young, S. G. Kukolich, J. Mol. Spec. 114, 483, 1985.

[76] S. Li, M-K. Park, C. O. Jo, S. Park, J. Atmos. 74, 227, 2017.

[77] S. L. Miller, L. C. Aamodt, G. Dousmanis, C. H. Townes, J. Kraitchman, J. Chem. Phys. 20, 1112, 1952.

[78] S. Solomon, Rev. of Geophys. 37, 275, 1999.

[79] S. Q. D. A.Filho, A. M. F. Costa, I. H. S. Ribeiro, R. Custodio, D. H. Pereira, Comp. Theo. Chem., 112589, 1166, 2019.

[80] Texas Advanced Computing Center (TACC) The University of Texas at Austin

[81] T. H. Dunning Jr., P. J. Hay, Gaussian Basis Set for Molecular Calculations in Methods of Electronic Structure Theory, Ed. Schaefer III, H.F., Modern Theoretical Chemistry, Vol. 3 Plenum New York, pp. 1-28, 1976.

[82] T. H. Raymond, S. R. Rajiv, S. J. George, I. Shankland, D. P. Wilson, R. P. Robinson, M. V. D. Puy, J. L. Welch, G. J. Shafer, M. W. Spatz, R.Hulse, "Use of Low GWP Refrigerants Comprising $CF_3I$ with Stable Lubricants". 2011.

[83] "The Montreal Protocol on Substances That Deplete the Ozone Layer - United States Department of State" U.S. Department of State, https://www.state.gov/key-topics-office-of-environmental-quality-and-transboundary-issues/the-montreal-protocol-on-substances-that-deplete-the-ozone-layer/, April 5, 2019.Accessed March 10, 2020.

[84] T. J. Balle, W. H. Flygare, Rev. Sco. Instrum. 52, 33, 1981.

[85] T. Kasuya, T. Oka, J. Phys. Soc. Jap. 2, 15, 1960.

[86] T.Kistemann, J. Hundhausen, S. Herbst, T. Claben, H. Färber, Inter. J. Hygiene Environ. Health, 211, 308, 2008.

[87] T. N. Tanada, J. Velazquez, N. Hemmi, T. A. Cool, Ber. Bungsenges. Phys. Chem., 97, 1516, 1993.

[88] United Nations Environment Programme (UNEP), 2003. Handbook for the International Treaties for the Protection of the Ozone Layer, Nairobi, Kenya. Available at. http:// www.unep.org/Ozone/pdfs/Handbook-2003.pdf.

[89] V. Fock, Zeitschrift Für Physik, 62, 795, 1930.

[90] W. Gordy, R. L Cook, Microwave Molecular Spectra, Interscience Publishers, Inc.1970

[91] W. Gordy, J. W. Simmons, and A. G. Smith, Phys. Rev. 3, 74, 1948.

[92] W. H. Flygare and W. D. Gwinn, J. Chem. Phys. 36, 787, 1962.

[93] W. H. Flygare, J. of Mol. Spec. 14, 145, 1964.

[94] W. Jäger, FTMW Spectroscopy, http://www.chem.ualberta.ca/~jaeger/research/ftmw/ftmw.htm, March 24,2020.

[95] W. L. Chameides, D. D. Davis, J. Geophys. Resear. 85, 7383, 1980.

[96] W. Lin, Fourier Transform Microwave Spectroscopy of Scandium Monohalides, Thesis, University of British Columbia, 1999.

[97] WMO, W. "Scientific assessment of ozone depletion: 2006." *World Meteorological Organisation, Global Ozone Research and Monitoring Project–Report* 50, 2007.

[98] W. ReifenHäuser, K. G. Heumann, Atmo. Enviro. Part A, Gen. Topic, 26, 2905, 1992.

[99] W. Stahl, H. Dreizler, M. Hayashi, Z. Natur. 38a, 1010, 1983.

[100] W. Tsang, Combust. Sci. and Tech. 74, 99, 1990.

[101] Y. Endo, High-Resolution Spectroscopic Studies of Reaction Intermediates Relevant to Atmospheric Chemistry, International Symposium on Molecular Spectroscopy, https://slideplayer.com/slide/5978787/, 2014

[102] Y. L. Yung, J. P. Pinto, R. T. Watson, S. P. Sander, J. Atmos. Sci. 37, 339, 1980.

[103] Z. Kisiel, L. Pszczól, W. Caminati, O. Favero, J. Chem. Phys. 105, 1778, 1996.

[104] Z. Kisiel, L. Pszczól, W. Caminati, O. Favero, J. Mol. Spec. 189, 283, 1998.

[105] Z. Kisiel, Rotational Spectroscopy Links, http://www.ifpan.edu.pl/~kisiel/rotlinks, March 2, 2020.

# APPENDIX A

## Maria Procedure

Start up:

1. Turn on both power bars. Check the “Fans” light (green one) to make sure it is on.
2. Turn on the turbo pump from the side (it will start with a self-check for about 30 seconds)
3. After the self-check, turn on the pump by pressing the power on button. (it will take from 10 to 15 mins to pump down to desired vacuum level. (when you see 309: 1500 Hz) and pressure reading at around 0.
4. While waiting for the system to pump down, turn on the laptop computer
5. Click on the app “8 PI control Panel” and wait until it is fully loaded.
6. Click on the app “Edgar mmWave”
7. Make sure that you can see “ready” at the bottom of program interface before starting the measurements.

Shut down:

1. After making sure you have saved all of the data, close the Edgar mmWave program.
2. Close the app “8 PI control Panel”
3. Close any remaining app.
4. Close the valve connecting to the sample vial, then open up the needle valve slowly to pump down any remaining sample in the gas line.
5. Turn off the pump by pressing the power off button (the same as power on button), you will see the increasing pressure reading. Wait until it states 309: 0Hz, it takes about 10 min)
6. Turn off the vacuum pump from the side.
7. Turn off both power bars.

***Static mode*** (this is only if you sample has extremely low vapor pressure)

1. While the sample and needle valve are completely open and your pressure meter is marking 00.00 mtorr (or extrmely low).
2. Flip the switch located on the left side of the pressure meter and below the sample cell to “off”. **( you should hear a clik sound arising from the angle valve)**
3. Begin a timer for 15 minutes *as you have a maxium of 20 minutes for static mode.* (**Pushing more than 20 minutes can cause damage to the turbo pump)**
4. The pressure should begin to rise. (**The pressure should reach a maximum of 10 mtorr).**

5. This can be controlled by closing the needle valve, which wont allow any sample to come go into the sample cell.
6. After 1-2 minutes begin running measurements.
7. Once done with measurements, make sure that the needle valve and sample valve are closed completely.
8. Once done, flip the switch to “on” **(you should hear a click)**
9. You are done, repeat if needed.

# APPENDIX B

## Sequential Coupling Scheme

### B.1

Below is the filename.par file used for fitting.

```
1,1-diiodoethane      Thu May 23 1Tue Jun 04 11:22:12 2019
  18   78    8    0    0.0000E+000    4.0000E+022    1.0000E+000
1.0000000000
a   66    1    0   12    0   -3    1    1         0   -1
10000  4.476339277534789E+003 1.00000000E+037 /A
20000  6.068741595522226E+002 1.00000000E+037 /B
30000  5.694102892760241E+002 1.00000000E+037 /C
200 -2.308657457976916E-001 1.00000000E+037 /DJ
1100  1.341688326676811E+000 1.00000000E+037 /DJK
2000  1.311984069337918E+001 1.00000000E+037 /DK
40100 -1.800884221818424E-001 1.00000000E+037 /dJ
41000  7.418922380115690E+000 1.00000000E+037 /dK
110010000 -1.636317829083909E+003 1.00000000E+037 /3/2Chi_aa
-220010000 -1.636317829083909E+003 1.00000000E-037 /3/2Chi_aa
110040000 -1.366542862769735E+002 1.00000000E+037 /1/4Chi_bb-
-220040000 -1.366542747761183E+002 1.00000000E-037 /1/4Chi_bb-
110210000  3.399470305405217E+002 1.00000000E+037 /Chi_bc
-220210000  3.399470305405217E+002 1.00000000E-037 /Chi_bc
110410000  5.439919468996119E+002 1.00000000E+037 /Chi_ac
-220410000 -5.439919468996119E+002 1.00000000E-037 /Chi_ac
110610000 -1.195646740074121E+003 1.00000000E+037 /Chi_ab
-220610000  1.195646740074121E+003 1.00000000E-037 /Chi_ab
```

B.2

Below shows the .lin file. This file contains all the recorded rotational transitions that were utilized to provide the seqential fit.

```
 2  2  1  5  7  1  1  0  5  6           14120.230     .005

 2  2  1  4  6  1  1  0  4  5           14134.273     .005

 2  2  1  4  5  1  1  0  4  4           14151.016     .005

 2  2  1  5  5  1  1  0  5  5           14156.436     .005

 2  2  0  5  5  1  1  0  5  5           14157.856     .005

 2  2  1  1  3  1  1  0  3  2           14160.248     .005

 2  2  0  2  3  1  1  1  2  2           14161.347     .005

 2  2  0  4  6  1  1  1  4  5           14247.629     .005

 2  2  0  2  4  1  1  1  2  3           14251.105     .005

 2  2  1  4  5  1  1  0  4  5           14270.207     .005

 2  2  0  3  5  1  1  1  3  4           14276.216     .005

 2  2  1  5  5  1  1  0  3  4           14351.745     .005

 2  2  0  5  4  1  1  1  3  4           14352.715     .005

 2  2  0  4  3  1  1  1  4  3           14353.223     .005

 2  2  0  4  5  1  1  1  4  4           14359.468     .005

 2  2  0  5  4  1  1  1  3  3           14362.998     .005

 2  2  0  4  5  1  1  1  4  5           14385.152     .005

 2  2  1  1  3  1  1  0  3  3           14400.699     .005

 2  2  0  1  3  1  1  1  3  2           14458.590     .005

 2  2  1  5  6  1  1  0  5  6           14471.324     .005

 2  2  0  5  5  1  1  1  5  5           14471.758     .005

 2  2  0  4  4  1  1  1  4  4           14479.211     .005

 2  2  0  4  4  1  1  1  4  3           14481.977     .005

 2  2  0  5  6  1  1  1  5  6           14525.572     .005

 2  2  1  5  5  1  1  1  5  4           14589.004     .005

 3  2  2  3  6  2  1  1  3  5           15169.782     .005
```

| | | | | | | | | | | | |
|---|---|---|---|---|---|---|---|---|---|---|---|
| 3 | 2 | 2 | 4 | 7 | 2 | 1 | 1 | 4 | 6 | 15212.157 | .005 |
| 3 | 2 | 2 | 5 | 8 | 2 | 1 | 1 | 5 | 7 | 15229.943 | .005 |
| 3 | 2 | 2 | 4 | 5 | 2 | 1 | 1 | 4 | 5 | 15255.323 | .005 |
| 3 | 2 | 2 | 5 | 7 | 2 | 1 | 1 | 5 | 6 | 15324.092 | .005 |
| 3 | 2 | 2 | 2 | 3 | 2 | 1 | 1 | 0 | 2 | 15326.229 | .005 |
| 3 | 2 | 1 | 5 | 2 | 2 | 1 | 2 | 5 | 3 | 15331.999 | .005 |
| 3 | 2 | 1 | 5 | 8 | 2 | 1 | 2 | 5 | 7 | 15407.764 | .005 |
| 3 | 2 | 1 | 5 | 5 | 2 | 1 | 2 | 5 | 4 | 15440.932 | .005 |
| 3 | 2 | 2 | 4 | 5 | 2 | 1 | 2 | 2 | 4 | 15454.743 | .005 |
| 3 | 2 | 1 | 4 | 4 | 2 | 1 | 2 | 2 | 4 | 15464.199 | .005 |
| 3 | 2 | 1 | 4 | 7 | 2 | 1 | 2 | 4 | 6 | 15486.753 | .005 |
| 3 | 2 | 1 | 3 | 6 | 2 | 1 | 2 | 3 | 5 | 15504.003 | .005 |
| 3 | 2 | 1 | 3 | 5 | 2 | 1 | 2 | 3 | 4 | 15579.200 | .005 |
| 3 | 2 | 1 | 4 | 6 | 2 | 1 | 2 | 4 | 5 | 15596.401 | .005 |
| 3 | 2 | 1 | 5 | 6 | 2 | 1 | 2 | 5 | 6 | 15665.564 | .005 |
| 3 | 2 | 1 | 5 | 7 | 2 | 1 | 2 | 5 | 6 | 15679.752 | .005 |
| 3 | 2 | 1 | 2 | 3 | 2 | 1 | 2 | 0 | 2 | 15703.391 | .005 |
| 3 | 2 | 1 | 3 | 4 | 2 | 1 | 2 | 3 | 3 | 15715.407 | .005 |
| 3 | 2 | 1 | 4 | 5 | 2 | 1 | 2 | 4 | 4 | 15716.453 | .005 |
| 3 | 2 | 1 | 5 | 6 | 2 | 1 | 2 | 5 | 5 | 15721.157 | .005 |
| 3 | 2 | 1 | 3 | 6 | 2 | 1 | 2 | 5 | 5 | 15729.232 | .005 |
| 5 | 2 | 4 | 5 | 8 | 4 | 1 | 3 | 5 | 8 | 17385.525 | .005 |
| 5 | 2 | 4 | 5 | 3 | 4 | 1 | 3 | 5 | 2 | 17396.240 | .005 |
| 5 | 2 | 4 | 4 | 7 | 4 | 1 | 3 | 4 | 7 | 17410.373 | .005 |
| 5 | 2 | 4 | 5 | 4 | 4 | 1 | 3 | 5 | 3 | 17423.135 | .005 |
| 5 | 2 | 4 | 1 | 6 | 4 | 1 | 3 | 1 | 5 | 17445.362 | .005 |
| 5 | 2 | 4 | 5 | 7 | 4 | 1 | 3 | 5 | 7 | 17451.432 | .005 |
| 5 | 2 | 4 | 1 | 6 | 4 | 1 | 3 | 5 | 6 | 17451.946 | .005 |

| | | | | | | | | | | | |
|---|---|---|---|---|---|---|---|---|---|---|---|
| 5 | 2 | 4 | 1 | 5 | 4 | 1 | 3 | 1 | 4 | 17455.539 | .005 |
| 5 | 2 | 4 | 2 | 5 | 4 | 1 | 3 | 2 | 4 | 17455.871 | .005 |
| 5 | 2 | 4 | 5 | 7 | 4 | 1 | 3 | 5 | 6 | 17458.260 | .005 |
| 5 | 2 | 4 | 0 | 5 | 4 | 1 | 3 | 0 | 4 | 17458.328 | .005 |
| 5 | 2 | 4 | 3 | 5 | 4 | 1 | 3 | 3 | 4 | 17458.693 | .005 |
| 5 | 2 | 4 | 5 | 8 | 4 | 1 | 3 | 5 | 7 | 17465.297 | .005 |
| 5 | 2 | 4 | 4 | 7 | 4 | 1 | 3 | 4 | 6 | 17466.209 | .005 |
| 5 | 2 | 4 | 5 | 6 | 4 | 1 | 3 | 5 | 5 | 17468.010 | .005 |
| 5 | 2 | 4 | 4 | 5 | 4 | 1 | 3 | 4 | 4 | 17471.377 | .005 |
| 5 | 2 | 4 | 5 | 9 | 4 | 1 | 3 | 5 | 8 | 17472.168 | .005 |
| 5 | 2 | 4 | 2 | 4 | 4 | 1 | 3 | 2 | 3 | 17480.074 | .005 |
| 5 | 2 | 4 | 1 | 4 | 4 | 1 | 3 | 1 | 3 | 17485.065 | .005 |
| 5 | 2 | 4 | 5 | 10 | 4 | 1 | 3 | 5 | 9 | 17489.468 | .005 |
| 5 | 2 | 4 | 2 | 6 | 4 | 1 | 3 | 2 | 5 | 17498.815 | .005 |
| 5 | 2 | 4 | 3 | 6 | 4 | 1 | 3 | 3 | 5 | 17500.166 | .005 |
| 5 | 2 | 4 | 4 | 8 | 4 | 1 | 3 | 4 | 7 | 17501.338 | .005 |
| 5 | 2 | 4 | 3 | 5 | 4 | 1 | 3 | 1 | 5 | 17504.032 | .005 |
| 5 | 2 | 4 | 4 | 2 | 4 | 1 | 3 | 4 | 1 | 17505.980 | .005 |
| 5 | 2 | 4 | 3 | 3 | 4 | 1 | 3 | 3 | 2 | 17508.891 | .005 |
| 5 | 2 | 4 | 3 | 3 | 4 | 1 | 3 | 3 | 2 | 17511.035 | .005 |
| 5 | 2 | 4 | 3 | 7 | 4 | 1 | 3 | 3 | 6 | 17513.568 | .005 |
| 5 | 2 | 4 | 2 | 7 | 4 | 1 | 3 | 2 | 6 | 17520.821 | .005 |
| 5 | 2 | 4 | 4 | 9 | 4 | 1 | 3 | 4 | 8 | 17527.473 | .005 |
| 5 | 2 | 4 | 3 | 8 | 4 | 1 | 3 | 3 | 7 | 17529.072 | .005 |

B.3

Below shows the sequential fit file, filename.fit.

```
            NEW PARAMETER (EST. ERROR) -- CHANGE THIS ITERATION
1         10000          A         4476.277(176)   -0.062
  2         20000          B        606.869( 34)   -0.006
  3         30000          C        569.4077(126)  -0.0026
  4           200         DJ         -0.23089( 37) -0.00002
  5          1100        DJK          1.34221(166)  0.00052
  6          2000         DK         13.132( 34)    0.012
  7         40100         dJ         -0.180082(179) 0.000006
  8         41000         dK          7.4196( 74)   0.0007
  9     110010000  3/2Chi_aa      -1636.3174(135)   0.0004
 10     110040000 1/4Chi_bb-       -136.6541( 37)   0.0002
 11     110210000     Chi_bc        339.9492(145)   0.0022
 12     110410000     Chi_ac        543.995( 40)    0.003
 13     110610000     Chi_ab      -1195.6407(299)   0.0061
MICROWAVE AVG =0.000665 MHz, IR AVG =0.00000
MICROWAVE RMS =0.778970 MHz, IR RMS =0.00000
END OF ITERATION  8 OLD, NEW RMS ERROR= 155.79400   155.05216
```

# BIOGRAPHICAL SKETCH

Michael Joseph Carrillo, who resides at 4523 Dei Gratia Dr. Brownsville, Tx. 78521. In July 2020 he earned his Master of Science in Chemistry. He earned his Bachelor of Science in Chemistry in December 2017. He attended IDEA Frontier College Preparatory, where he graduated in May 2013. After his undergraduate study, he shortly worked for Federal Express while waiting to get into his graduate studies. Once he was accepted into his graduate studies, he continued working in the laboratory of Prof. Wei Lin, whom he had conducted research with for 6 years. Michael's research interest is in microwave spectroscopy and has been for the last 6 years. He has been fortunate to present his research findings at several local symposiums, like the engaged scholar symposium and national symposiums like the 2016 and 2017 Annual Biomedical Research Conference for Minority Students, the 253rd American Chemical Society National Meeting located in San Francisco, and the 26th Austin Symposium on Molecular Dynamics at Dallas. He will continue to pursue his dream goal of obtaining his Ph.D. in Chemistry.